Biostratigraphy and Microfacies of Upper Cretaceous Oceanic Red Beds in the Northern Tethyan Himalaya: A Case Study from the Zhangguo Section, Gyangze, Southern Tibet, China

Yuewei Li , Guobiao Li * , Jie Ding , Dan Xie , Tianyang Wang , Zhantu Baoke , Mengmeng Jia , Chengshan Wang

Posted Date: 18 April 2025

doi: 10.20944/preprints202504.1520.v1

Keywords: CORBs; planktic foraminiferal biostratigraphy; microfacies, Late Cretaceous; Zhangguo; Tibet

 doi:10.20944/preprints202504.1520.v1

Article

Biostratigraphy and Microfacies of Upper Cretaceous Oceanic Red Beds in the Northern Tethyan Himalaya: A Case Study from the Zhangguo Section, Gyangze, Southern Tibet, China

Yuewei Li [1,2,3], Guobiao Li [1,2,*], Jie Ding [1,2], Dan Xie [3], Tianyang Wang [1,2], Zhantu Baoke [1,2], Mengmeng Jia [1,2] and Chengshan Wang [1,2]

[1] State Key Laboratory of Environmental Geology and Biogeology, China University of Geosciences, Beijing 100083, China
[2] School of Earth Sciences and Resources, China University of Geosciences, Beijing 100083, China
[3] Institute of Vertbrate Paleontology and Paleoanthropology, Chinese Academy of Sciences, Beijing 100044, China
* Correspondence: liguobiao@cugb.edu.cn

Abstract: The Cretaceous oceanic red beds (CORBs) and their implications for "oceanic oxic events" have been widely studied by geologists globally. In southern Tibet, CORBs are extensively distributed within the Upper Cretaceous strata of the northern Tethyan Himalaya (NTH). A well-exposed, CORB-bearing, mixed carbonate-shale sequence is found in the Zhangguo section of Rilang Township, Gyangze County. The Chuangde Formation in this section is characterized by well-preserved CORBs, which include reddish shale, limestone, marlstone, and interbedded siltstone. These CORBs are stratigraphically overlain by the Jiabula/Gyabula Formation (predominantly shale) and underlain by the Zongzhuo Formation ("mélange"). However, the precise age, depositional environments, and regional/global correlations of these CORBs, as well as their implications for synchronous versus diachronous oceanic oxic events, remain to be fully understood. In this study, a comprehensive analysis of foraminiferal biostratigraphy and microfacies is conducted for the CORB-bearing Chuangde Formation and the upper Jiabula (Gyabula) Formation in the Zhangguo section. Five planktic foraminiferal biozones including *Dicarinella asymetrica*, *Globotruncanita elevata*, *Contusotruncana plummerae*, *Radotruncana calcarata*, and *Globotruncanella havanensis* are identified through detailed biostratigraphic analysis, confirming a Campanian age for the Chuangde Formation and its CORBs. These findings are broadly correlated with typical Upper Cretaceous CORBs in pelagic-hemipelagic settings across the NTH in southern Tibet. Nine microfacies and four facies associations are identified within the Upper Cretaceous strata of Gyangze and adjacent areas through field and petrographic analyses. Notably, it is indicated that planktic foraminiferal packstone/grainstone CORBs were deposited in outer shelf to upper slope environments, while radiolarian chert CORBs are inferred to have formed in deep-water, basinal settings below the carbonate compensation depth (CCD).

Keywords: CORBs; planktic foraminiferal biostratigraphy; microfacies; Late Cretaceous; Zhangguo; Tibet

1. Introduction

Red beds, characterized by reddish hues due to iron oxides, are globally widespread sedimentary sequences formed under oxidizing conditions (Turner, 1980) [1]. Marine red beds (MRBs), found in marine settings, are distinct from continental red beds (CRBs) (Fischer and Arthur, 1977; Basu, 1982) [2,3]. MRBs are significant in sedimentology, paleoceanography, paleontology,

 doi:10.20944/preprints202504.1520.v1

paleoecology, and paleoclimatology, offering insights into Earth's redox history and climatic shifts (Fischer and Arthur, 1977; Wang et al., 2005; Li et al., 2021) [2,4,5].

First identified in the 19th century in the Mediterranean, Europe, and North Africa (Lyell, 1833) [6], MRBs were initially described lithologically. Mid-20th century advances linked their red coloration to hematite (Fe_2O_3) and oxidizing conditions. The late 20th century saw MRBs integrated into studies of Oceanic Anoxic Events (OAEs), carbon cycling, and mass extinctions (Jenkyns, 1976; Arthur et al., 1987) [7,8].

Since the 21st century, high-resolution geochemical techniques and numerical modeling have advanced MRB research, revealing their roles in paleoenvironmental reconstruction, plate tectonics, and biological evolution (Li et al., 2011; Rong et al., 2019) [9,10]. MRBs are categorized into oceanic (basin), deeper water (slope), and shallow water (shelf) types based on depositional environments (Wang et al., 2009; Li et al., 2021) [5,11].

Cretaceous Oceanic Red Beds (CORBs), first identified in the Carpathians and eastern Alps (Štúr, 1860; Gümbel, 1861) [12,13], are globally distributed in the Atlantic, Pacific, Indian, and Tethyan Oceans (Wagreich and Krenmayr, 2005; Wang et al., 2005) [4,14]. Their formation is linked to Late Cretaceous oceanic oxidation, iron cycle changes, global cooling, and sea-level fluctuations (Mansour and Wagreich, 2022) [15]. CORBs mark the transition from anoxic to oxic marine conditions (Wang et al., 2011) [16].

In the northern Tethyan Himalaya (NTH), CORBs are exposed as reddish limestones, marlstones, shales, siltstones, and radiolarian cherts, with key outcrops in Yamdrok Lake, Gyangze, Kangmar, Sakya, Gyirong, and Zanda (Figure 1). These deposits, dated from late Santonian to early Paleocene, exhibit a progressive east-to-west age trend (Wan and Ding, 2002; Wan et al., 2005; Li et al., 2011) [9,17,18].

This study aims to (1) analyze the well-preserved CORB sequence in the Zhangguo section (Gyangze, NTH), (2) establish stratigraphic correlations with global CORB deposits, and (3) evaluate the synchroneity and paleoceanographic implications of Upper Cretaceous CORB deposition.

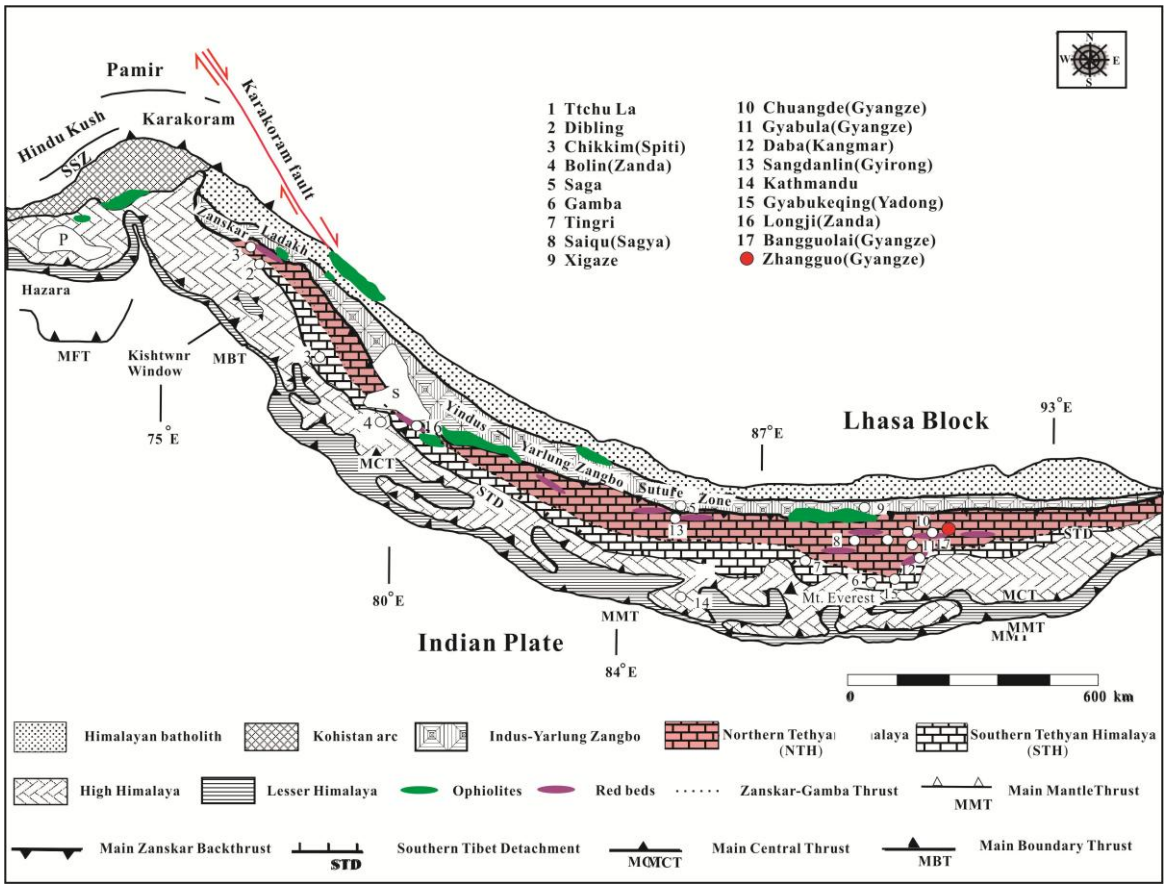

 doi:10.20944/preprints202504.1520.v1

Figure 1. Geological structure map of the Tethys Himalayas and its adjacent areas (The base map is after Gansser, 1964) [19] showing the sections with Cretaceous Oceanic Red Beds (CORBs) and location of the Zhangguo section in Gyangze, southern Tibet of China.

2. Materials and Methods

Detailed sedimentological study was carried out on the Upper Cretaceous strata, especially the CORBs, in the Zhangguo section (Coordinates 28°58′52″; N89°48′13″ E) of Rilang (Suokim/Suojin) town, Gyangze County, southern Tibet of China (Figure 2). A total of 112 samples of limestone, marlstone, shale, and silty sandstone (No. RB1 to RB112) were collected from the upper Jiabula (Gyabula), Chuangde (CORBs), and lowest Zongzhuo formations for biostratigraphic and microfacies analyses.

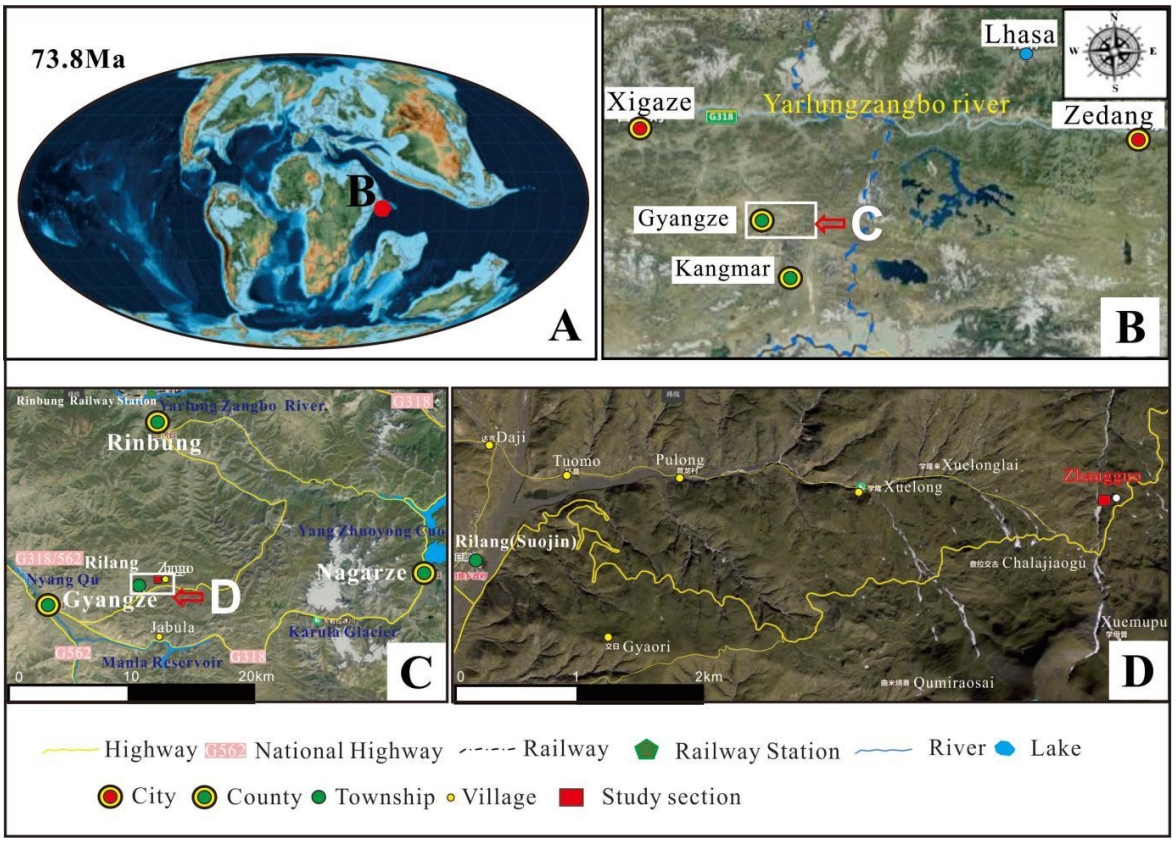

Figure 2. (**A**) Palaeogeographical location of the studied area (red dot) during the Late Campanian (~73.8 Ma). The base map is after Scotese (2021) [20] at http://www.serg.unicam.it/Intro- Reconstr.html. (**B**) Satellite image of the studied area in the vicinity of Xigaze, southern Tibet. (**C**) Detailed geographical map showing location of the studied section ("D") in Zhangguo, eastern Gyangze County (dash lines indicate the walking track). (**D**) Overview of the measured section covering the upper Gyabula, Chuangde, and lower Zongzhuo formations. [Colour figure can be viewed at wileyonlinelibrary.com].

Biostratigraphic analysis primarily relied on planktonic foraminifera, which were extracted from marlstones and limestones using the grinding method, which involved cutting rock samples into thin sections. A total of 34 thin sections, with particular emphasis on obtaining axial sections of foraminiferal tests, were subjected to detailed taxonomic examination. All specimens and corresponding rock samples are permanently housed at the Fossil Identification Center, China University of Geosciences (Beijing) (CUGB). While the foraminiferal preservation in the Zhangguo section exhibits varying degrees of recrystallization (Figures 3–10), the majority of specimens retain sufficient morphological integrity to permit reliable identification at both genus and species levels.

 doi:10.20944/preprints202504.1520.v1

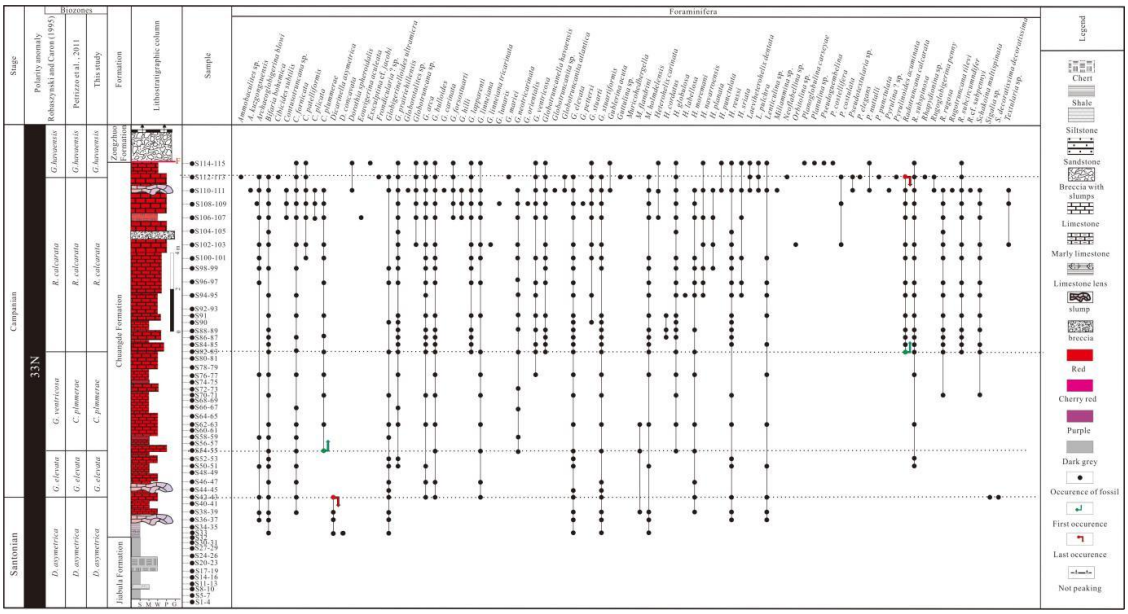

Figure 3. Stratigraphic column and ranges of planktic foraminifer species of the Upper Cretaceous strata in the Zhangguo area. Note that four foraminiferal biozones including *Globotruncanita elevata*, *Contusotruncana plummerae*, *Radotruncana calcarata*, and *Globotruncanella havanensis* zones were identified from the study area.

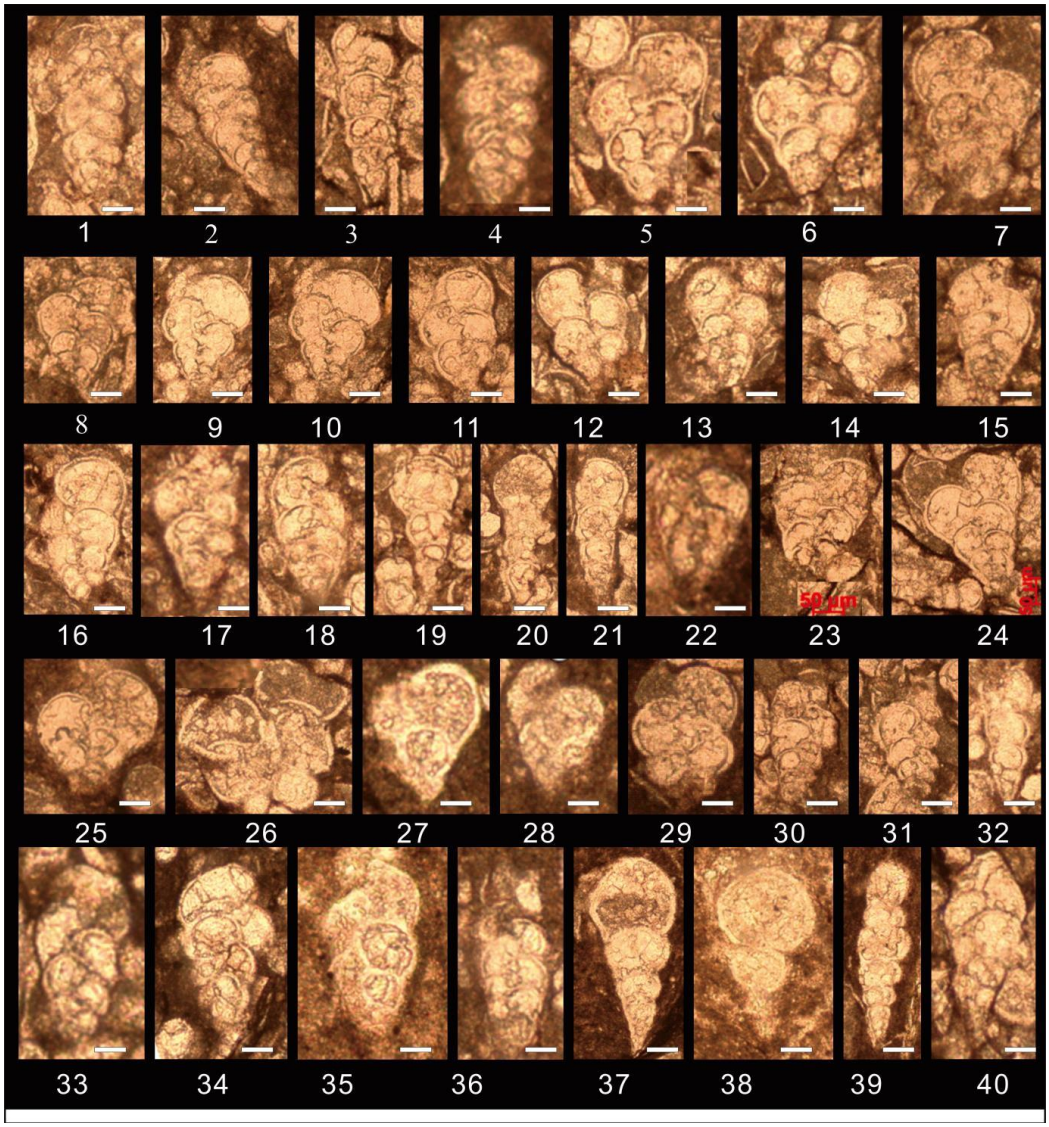

 doi:10.20944/preprints202504.1520.v1

Figure 4. Planktic foraminiferal species observed in thin sections from the Zhangguo section of Rilang, Gyangze County, southern Tibet of China. **1-3.** *Heterohelix moremani* (Cushman, 1938) (110); 4. *Heterohelix navarroensis* Loeblich, 1951 (115); 5-14. *Heterohelix reussi* (Cushman, 1938) (110); 15-21. *Heterohelix carinata* (Cushman, 1938) (15-20.110; 21. 115); 22. *Laeviheterohelix pulchra* (Brotzen, 1936) (115); 23, 24. *Heterohelix globulosa* (Ehrenberg, 1840) (112); 25. *Dorothia spheroidalis* Wan, 1985 (115); 26. *Dorothia* ? sp. (110); 27, 28. *Heterohelix cordites* Wan, 1985 (87); 29. *Heterohelix punctulata* (Cushman, 1938) (110); 30, 31. *Heterohelix carinata* (Cushman, 1938) (110); 32-34. *Heterohelix planata* (Cushman, 1938) (33. 110; 34, 35. 103); 35. *Heterohelix labellosa* (Nederbragt, 1991)(95); 36. *Heterohelix* cf. *navarroensis* Loeblich, 1951 (103); 37, 38. *Heterohelix globulosa* (Ehrenberg, 1840)(107); 39, 40. *Heterohelix moremani* (Cushman, 1938) (107; 110). White scale bar = 50 μm.

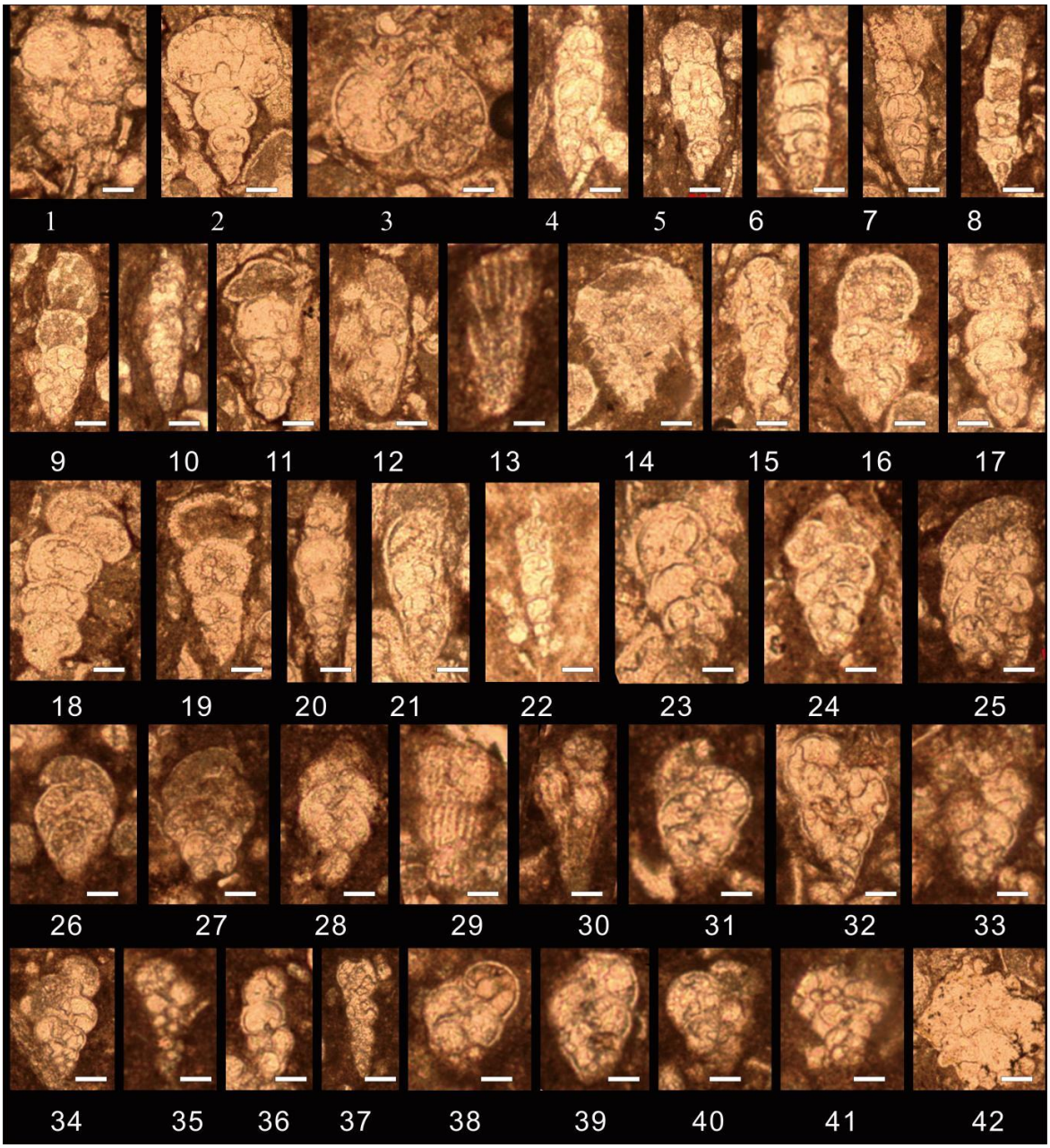

Figure 5. Biserial planktonic foraminifera from the Zhangguo section of Rilang, Gyangze County, southern Tibet of China. **1-3.** *Pseudotextularia nuttalli* (Voorwijk, 1937) (1.110; 2-3.115); 4-10. *Bifarina bohemica* (Sulc)(4-6. 110; 7. 112; 8, 9. 107; 10.103); 11. *Bifarina* sp.(112); 12, 13. *Pseudoguemblina costulata* (Cushman, 1938)(112; 103); 14, 15. *Eouvigerina aculeata* (Ehrenberg) (107); 16, 29, 30. *Heterohelix striata* (Ehrenberg, 1840) (107; 110; 115); 17, 18. *Pseudotextularia* sp. (110; 112); 19. *Pseudotextularia punctulata* (Cushman, 1938) (112); 20-22. *Bifarina bohemica* (Sulc) (20-21.112; 22. 102); 23, 24. *Heterohelix carinata* (Cushman, 1938) (107; 110); 25. *Pseudoguembelina costellifera*

 doi:10.20944/preprints202504.1520.v1

Masters, 1976(115); 26, 27. *Laeviheterohelix dentata* (Stenestad, 1968) (115); 28. *Laeviheterohelix pulchra* (Brotzen, 1936) (115); 31-34. *Heterohelix reussi* (Cushman, 1938) (115); 35. *Planoglobulina carseyae* (Plummer, 1931) (115); 36, 37. *Bifarina bohemica* (Sulc(115); 38-40. *Heterohelix punctulata* (Cushman, 1938) (115); 41, 42. *Gublerina acuta* De Klasz 1953 (115; 110). White scale bar = 50 μm.

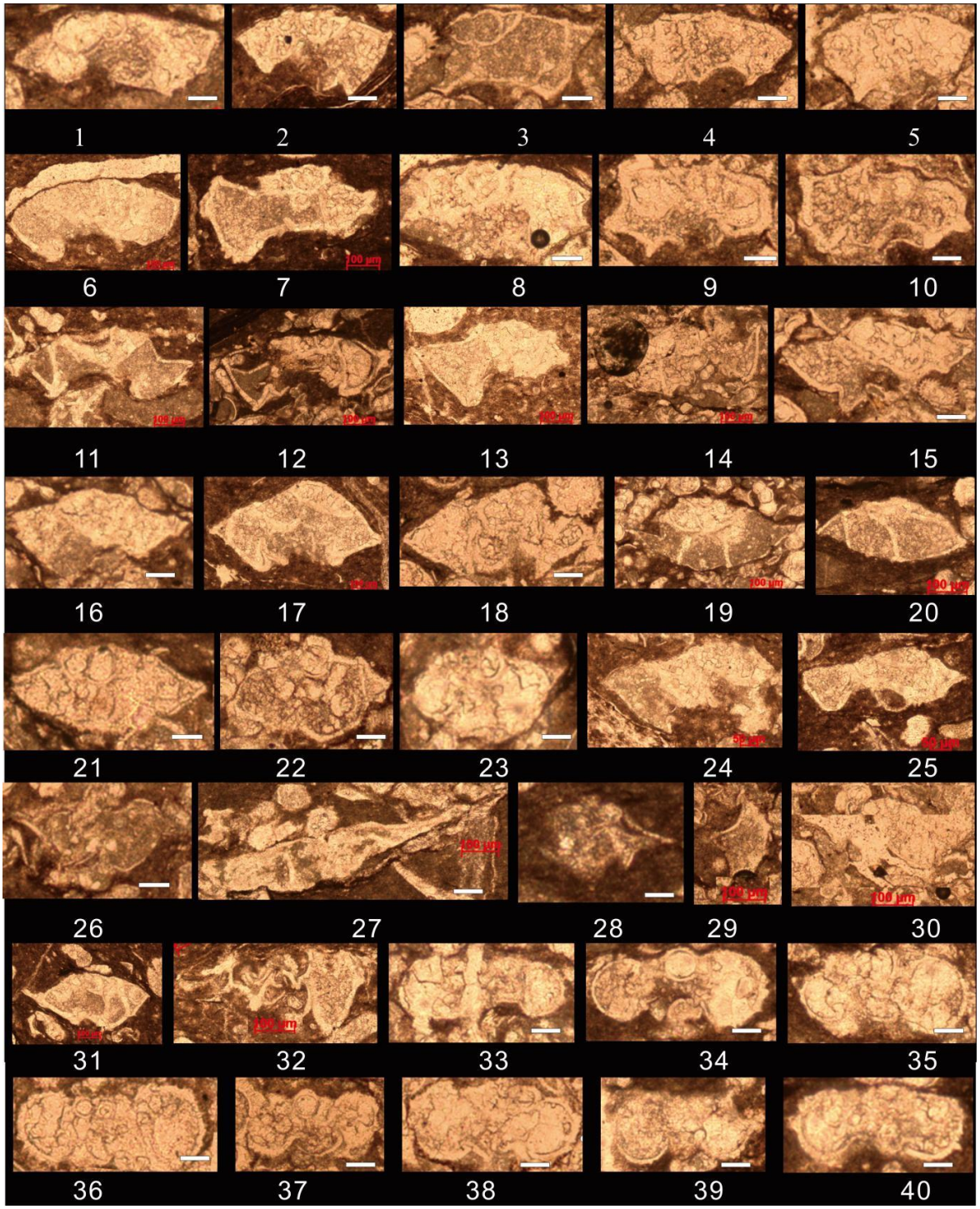

Figure 6. Trochospiral planktonic foraminifera from Zhangguo section of Rilang, Gyangze County, southern Tibet of China. **1-6.** *Globotruncanita stuarti* (Lapparent, 1918) (1. 112; 2. 109; 3-5.115; 6. 109); 7. *Globotruncana bulloides* Volgler, 1941 (110); 8-10. *Globotruncana ventricosa* White, 1928（109; 112; 112); 11-14. *Globotruncanita elevata* (Brotzen, 1934) (109; 110; 109; 110); 15, 16. *Globotruncanita stuartiformis* (Dalbiez, 1955) (110); 17-18. *Globotruncanita atlantica* (Caron, 1972)(110; 109); 19-21. *Globotruncanita stuarti* (Lapparent, 1918) (110); 22, 23. *Globotruncanita* sp. (110); 24, 25. *Globotruncanita* cf. *stuartiformis* (Dalbiez, 1955) (109; 100); 26-32. *Radotruncana*

 doi:10.20944/preprints202504.1520.v1

calcarata (Cushman, 1927) (26-30. 110; 31-32. 109); 33-40. *Archaeoglobigerina blowi* Pessagno, 1967 (112). White scale bar = 100 μm.

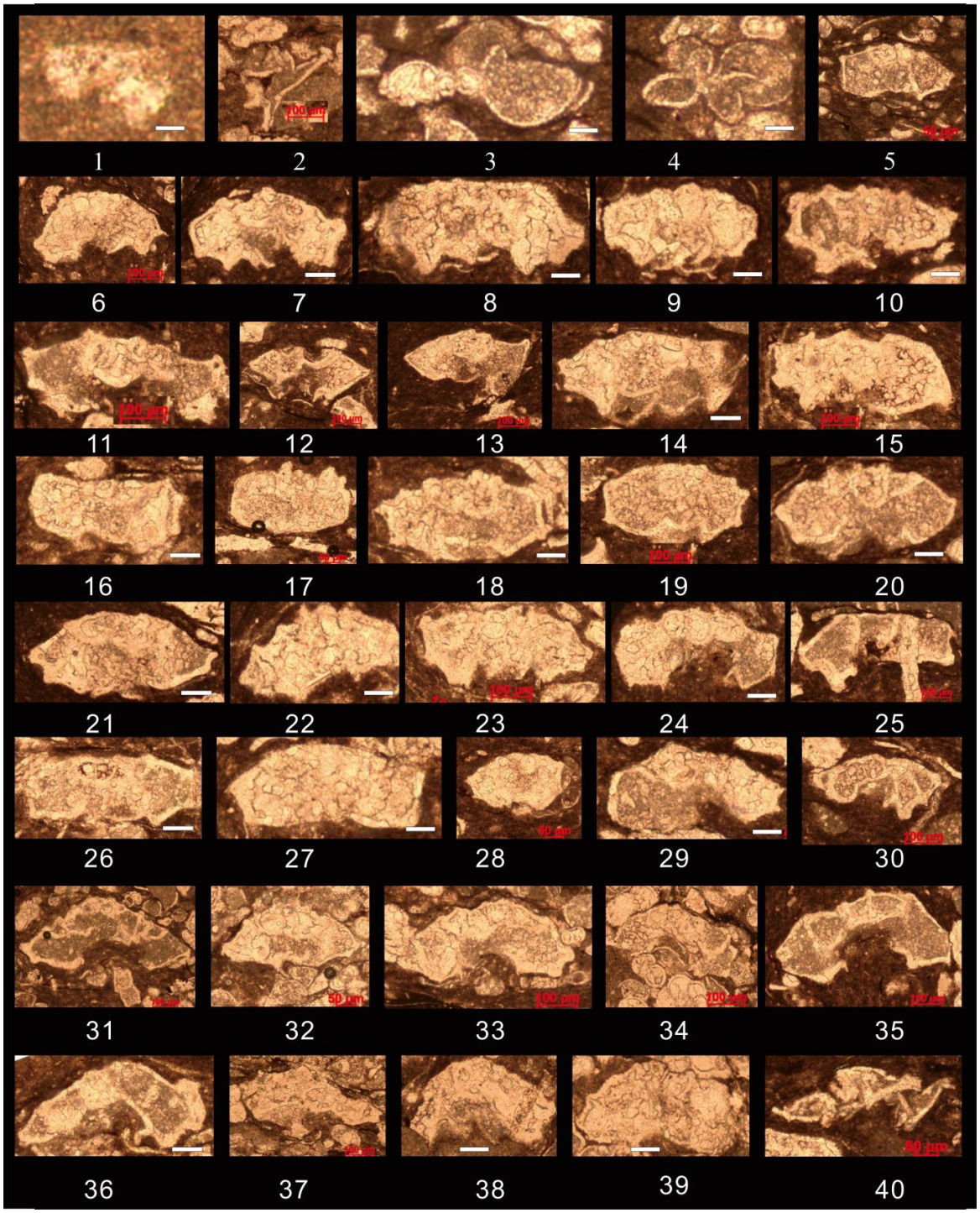

Figure 7. Trochospiral planktonic foraminifera from Zhangguo section of Rilang, Gyangze County, southern Tibet of China. ***1. Dicarinella asymetrica* (Sigal, 1952) (37); 2-4.** *Schakoina multispinata* (Cushman and Wickenden, 1930) (110; 103; 103); 5. *Globotruncana linneiana tricarinata* (Quereau, 1893) (103); 6-8. *Globotruncana arca* (Cushman, 1926) (103; 109; 109); 9-10. *Globotruncana lunaris* Masters, 1976 (109); 11. *Globotruncana lapparenti* Brotzen, 1936 (109); 12-13. *Globotruncanita pettersi* (Gandolf, 1955) (109); 14, 15. *Globotruncana* cf. *falsostuarti* Sigal, 1952 (110); 16-19. *Globotruncana hilli* Pessagno, 1967（110; 107; 109; 110); 20-21. *Globotruncana orientalis* El Naggar 1966 (109); 22-24. *Globotruncana arca* (Cushman, 1926 (22, 23. 109; 24. 110); 25-27. *Globotruncana lapparenti* Brotzen, 1936 (109); 27. *Globotruncana* cf. *lapparenti* Brotzen, 1936 (109); 28. *Globotruncana* cf. *hilli* Pessagno, 1967(110); 30. *Rugotruncana*

 doi:10.20944/preprints202504.1520.v1

subcircumndifer (Gandolfi, 1955) (109); 31, 32. *Globotruncanita atlantica* (Caron, 1972) (110); 33, 34. *Contusotruncana fornicata* (Plummer, 1931) (110); 35. *Contusotruncana patelliformis* (Gandolfi, 2003) (100); 36-38. *Contusotruncana plicata* (White 1928) (110); 39. *Contusotruncana plummerae* (Gandolfi, 1955) (110); 40. *Radotruncana calcarata* (Cushman, 1927) (109). White scale bar = 100 μm.

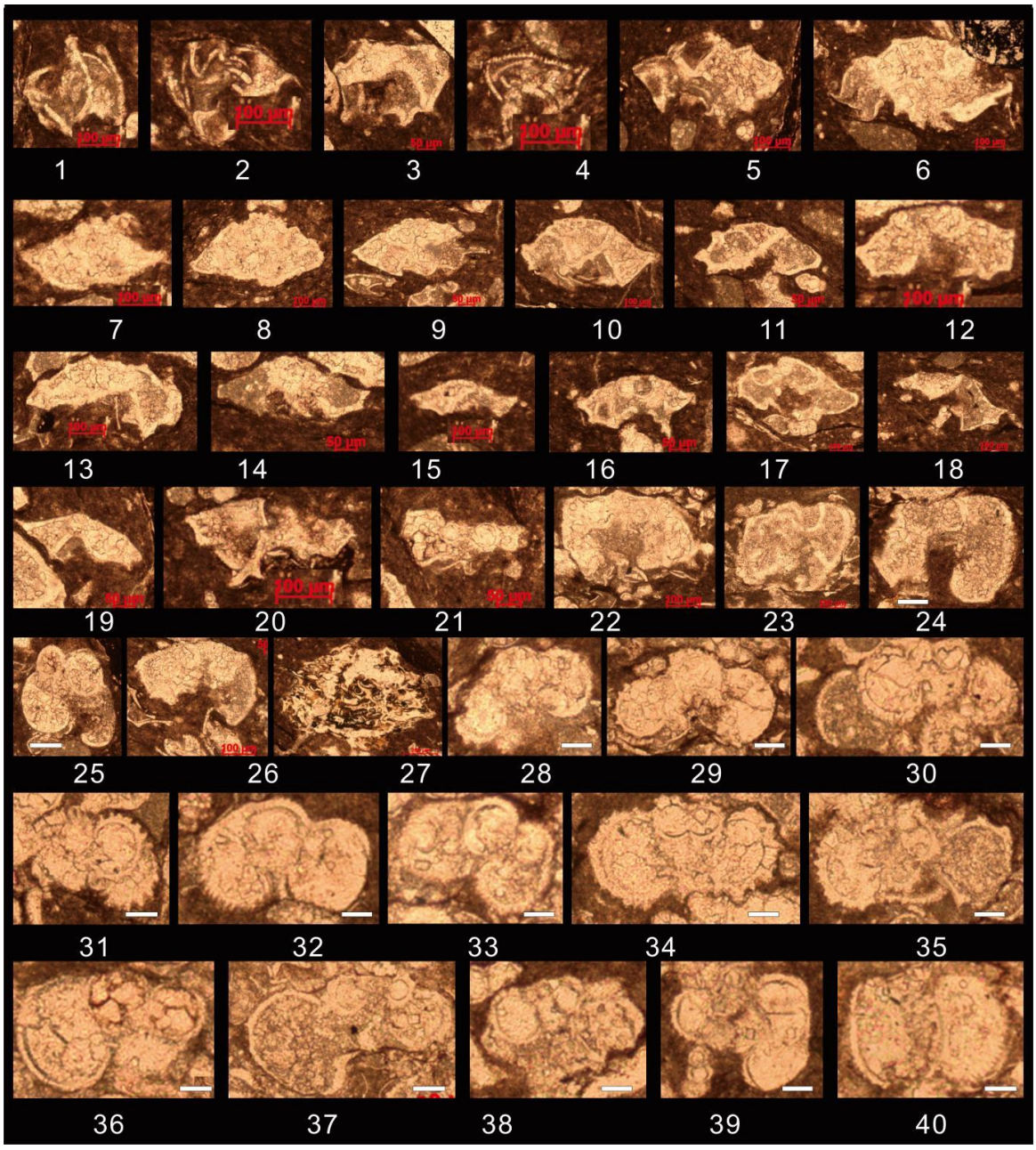

Figure 8. Trochospiral planktonic foraminifera from the Zhangguo section of Rilang, Gyangze County, southern Tibet of China. **1-3.** *Radotruncana calcarata* (Cushman, 1927) (109); 4. *Globotruncanita elevata* (Brotzen, 1934) (110); 5. *Globotruncanita stuartiformis* (Dalbiez, 1955) (109); 6. *Globotruncanita stuarti* (de Lapparent, 1918) (109); 7-9. *Globotruncana falsostuarti* Sigal, 1952 (109); 10-19. *Globotruncana arca* (Cushman, 1926) (109); 20, 21. *Rugotruncana subcircumndifer* (Gandolfi, 1955) (109); 22-24. *Contusotruncana* sp. Korchagin, 1982(110; 110; 107). 25. *Rugoglobigerina rugosa* (Plummer, 1926) (109); 26. *Rugotruncana subcircumndifer* (Gandolfi, 1955) (109); 27. *Globotruncanita* cf. *conica* (White, 1928) (109); 28-30. *Muricohedbergella holmdelensis* Olsson, 1964 (110); 31-33. *Rugoglobigerina penny* Brönnimann (110); 34, 35. *Rugotruncana tilevi* Brönnimann and Brown, 1956 (110); 36-38. *Rugoglobigerina rugosa* (Plummer, 1926) (112). 39, 40. *Rugoglobigerina pennyi* Bronnimann (112). White scale bar = 100 μm.

 doi:10.20944/preprints202504.1520.v1

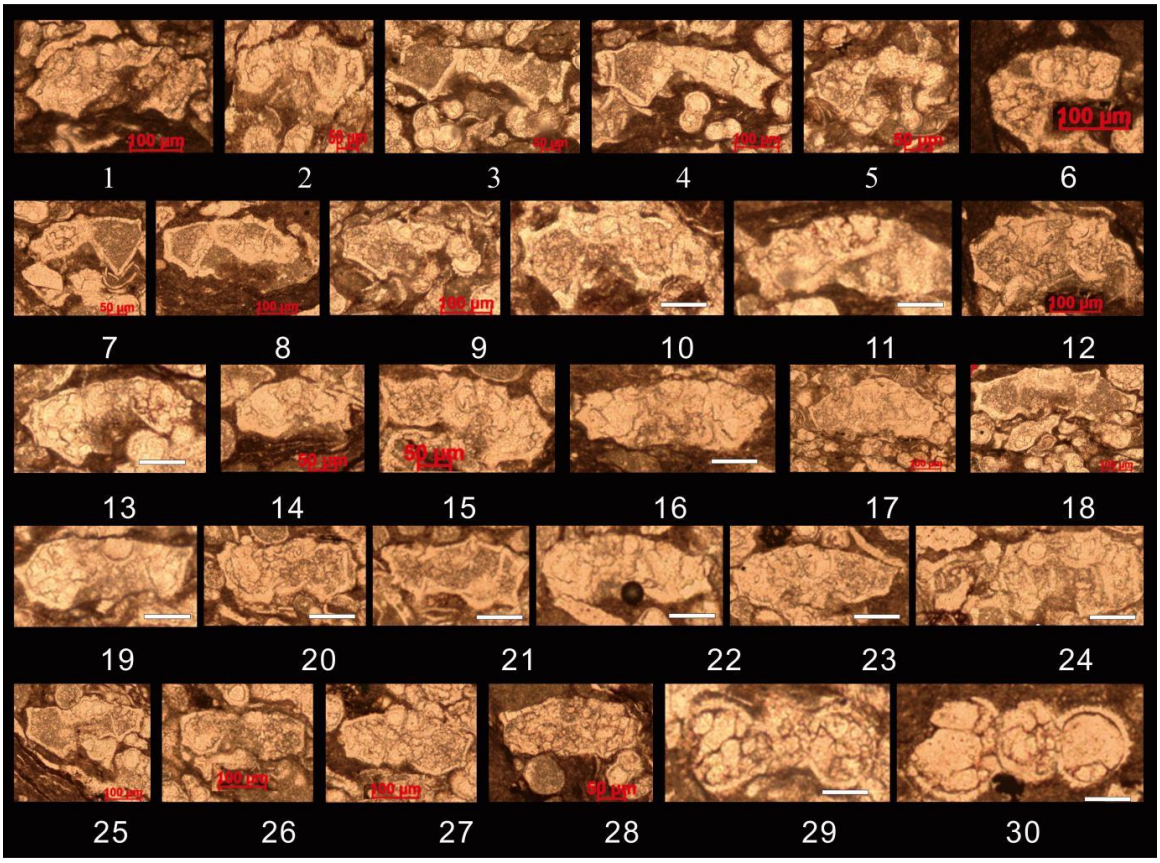

Figure 9. Trochospiral planktonic foraminifera from the Zhangguo section of Rilang, Gyangze County, southern Tibet of China. **1.** *Globotruncana neotricarinata* (Micro-Unimi n. 1983)(110); 2. *Rugotruncana* cf. *subpennyi* (Gandolfi, 1955) (110); 3-10. *Globotruncana ventricosa* White, 1928 (3-9. 110; 10. 109); 11-15. *Globotruncana arca* (Cushmani, 1926) (11-13. 110; 14, 15. 112); 20. *Globotruncana linneiana* (d'Orbigny, 1839) (110); 24-28. *Globotruncana lapparenti* Brotzen, 1936 (24, 25. 110; 26-28. 112); 29, 30. *Archaeoglobigerina blowi* Pessagno, 1967 (112). White scale bar = 100 μm.

Microfacies analysis was primarily conducted using thin sections. Carbonate rocks were classified according to their textures, following the classification scheme of Dunham (1962) [21]. Sedimentological interpretations of microfacies were based on field observations and textural characteristics, as outlined by Wilson (1975) [22] and Flügel (1972, 2010) [23,24]. The studied microfacies consist predominantly of limestones and cherts from the Zhangguo section in Gyangze (Figure 11). These were compared with microfacies from the Daba section in Kangmar (NTH) to assess variability in microfacies and changes in microfossils within CORBs.

 doi:10.20944/preprints202504.1520.v1

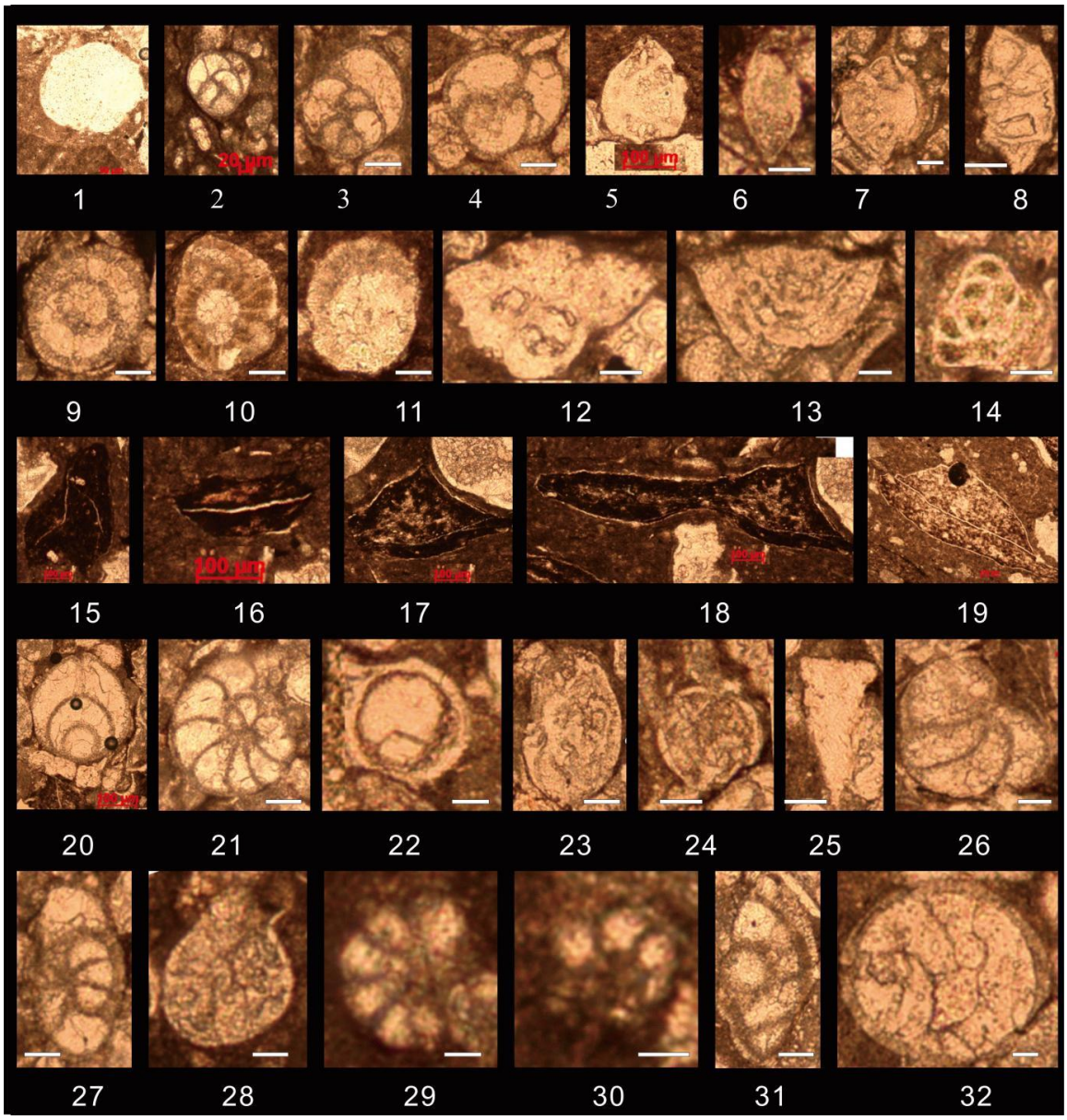

Figure 10. Benthic foraminifera from the Zhangguo section of Rilang, Gyangze County, southern Tibet of China. ***1.Orbitolina* sp.** d'Orbigny, 1850 (103); 2-4. *Textularia* sp. (103; 110; 110); 5. *Guttulina* sp. d'Orbigny, 1839 (112); 6-8. *Lenticulina* ? sp. (110); 9-12. Benthic foraminifers (110); 13. *Globorotalites* sp. Brotzen, 1942 (110); 14. *Miliammina* sp. Heron-Allen & Earland, 1930 (110); 15-20. Benthic foraminifers (112); 20. *Frondicularia* ? sp. Defrance, 1826 (112); 21. *Planulina* sp. d'Orbigny, 1826 (115); 22. *Neoflabellina* sp. (112); 23. *Cibicides subtilis* Zeng, 1982 (112); 24. *Pyrulinoides acuminata* (d'Orbigny) (112); 25. *Rhapydionina* sp. Stache, 1913 (112); 26. *Ammobaculites* sp. Cushman, 1910 (112); 27. *Ammobaculites kuzgongsuensis* Hao, 1982(110); 28. *Exsculptina* cf. *jacobi* (Marie) (115); 29, 30. *Lenticulina* sp. (115); 31. *Pyrulina* ? sp. d'Orbigny, 1839(110); 32. Ostricoda (112). White scale bar = 100 μm.

 doi:10.20944/preprints202504.1520.v1

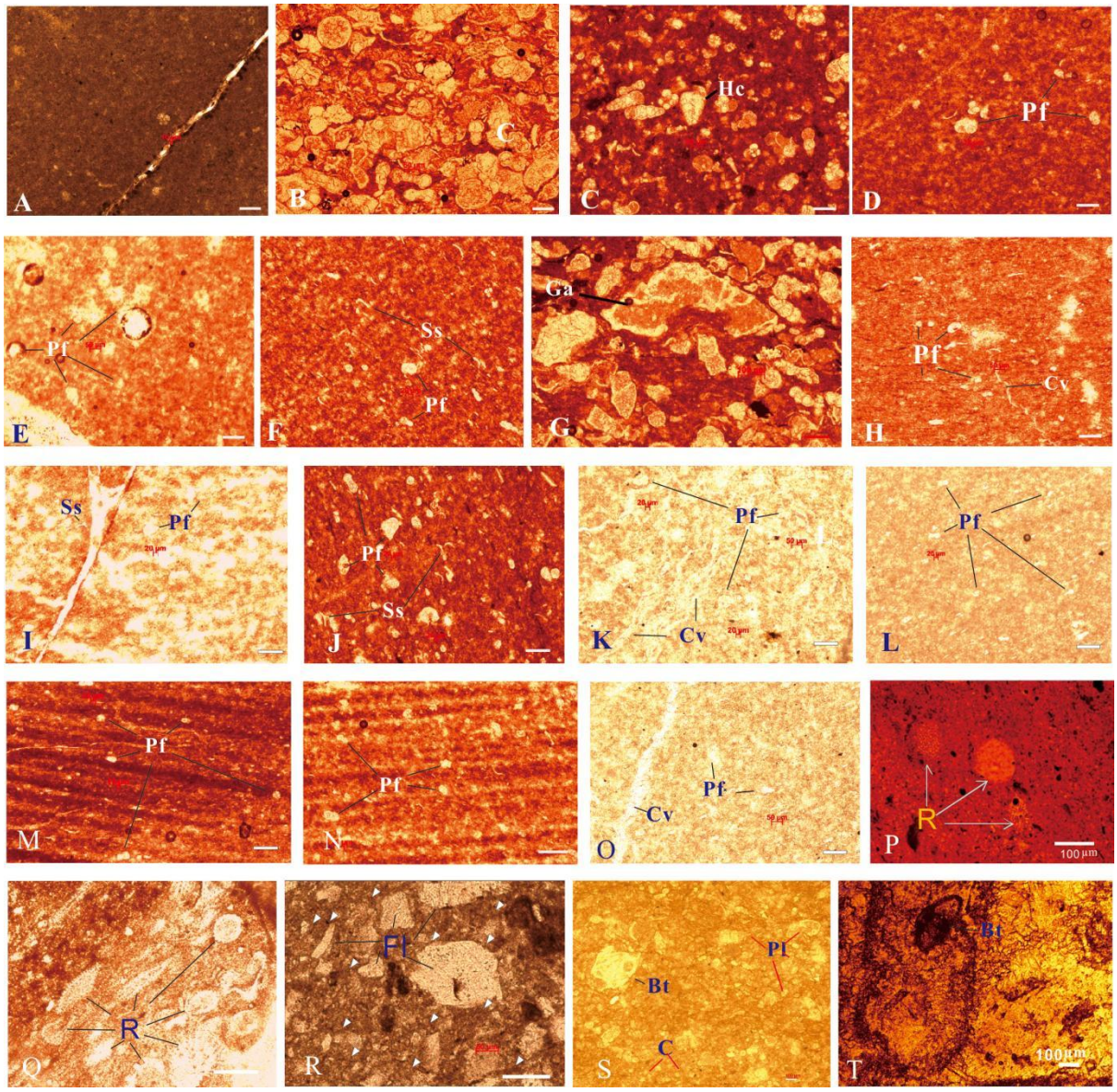

Figure 11. Photomicrographs showing the microfacies from the Upper Cretaceous Chuangde Formation in the Zhangguo secton of Gyangze (**A–O; R**), the Dada section of Kangmar (**P**), the Lari section of Zhongba (**Q**), and the Gyabukeqin (**S**) and Gulupu (**T**) sections of Yadong. **(A) Peloidal marlstone (MF 1; Sample No: S90).** Small, subrounded and subangular micritic grains. Poor sorting and distinct differences in size and shape indicate that these grains originated from the reworking of weakly lithified carbonate mud. The bright spot is portion of foraminiferal fossil. (**B**) Foraminiferal grainstone (MF6; S112). (**C**) Bioclastic wackestone with *Heterohelix carinata* (Hc) (MF3; S115). (**D**) Bioclastic wackestone with a few planktic foraminifera (Pf) (MF3; S95). (E) Loosely packed wackestone with planktic foraminifera (Pf) (MF4; S85). (**F**) Loosely packed wackestone with planktic foraminifera (Pf) and sponge spicule (Ss) (MF4; S99). (**G**) Planktic foraminiferal packstone with *Globotruncanita atlantica* (Ga) (MF5; S110). (**H**) Bioclastic wackestone (MF3; S42) with planktic foraminifera (Pf) and calcite veib (Cv). (**I**) Grainstone (MF6; S45) with planktic foraminifera (Pf) and sponge spicule (Ss), displaying "pane fabric". (**J**) Planktic foraminiferal packstone (MF5; S88) with planktic foraminifera (Pf) and Sponge spicule (Ss). (**K**) Grainstone (MF6; S37) with planktic foraminifera (Pf) and calcite veins (Cv). (**L**) Bioclastic packstone (MF5; S55) with planktic foraminifera (Pf). (**M**) Laminated packed wackestone (MF2; S53) with planktic foraminifera (Pf). (**N**) Laminated packed wackestone (MF2; S91) with planktic foraminifera (Pf). (**O**) Grainstone (MF6; S55) with planktic foraminifera (Pf) and calcite vein (Cv). (**P**) Radiolaria-bearing chert (MF7; 06DBwg059-1; Kangmar) with some radiolarians ("R"); (**Q**) Radiolarian siliceous rock (MF8; LR-C1; Zhongba) with abundant radiolarians ("R"). (**R**) Lithoclastic Wackestone/Floatstone (MF9; S104): Lithoclasts (floats) constitute over 60%, pressure

 doi:10.20944/preprints202504.1520.v1

solution stylolites (indicated by arrows) are clustered around the lithoclasts (floats) and are embedded within a micritic matrix; (**S**) Packstone with planktic (Pl) and benthic (Bt) foraminifera and calpionellids ("C") (MF5; K_2g110, Yadong); (**T**) Grainstone with benthic foraminifera (Bt) (MF6; YR5, Yadong). Scale bars represent 200 μm unless noted otherwise. [Colour figure can be viewed at wileyonlinelibrary.com].

3. Results

3.1. Planktic Foraminiferal Biostratigraphy

Abundant and well-preserved foraminiferal fossils were recovered from the Chuangde Formation (CORBs) in the Zhangguo section. Planktic foraminifera constitute the dominant elements of the analyzed assemblages, with the section's biostratigraphic framework primarily established through detailed foraminiferal analysis (Figures 3–10). Key diagnostic species were reliably determined through examination of fossil axial sections and rotary profiles.

The planktic foraminiferal assemblages are dominated by the following genera: Archaeoglobigerina, Bifarina, Contusotruncana, Dicarinella, Dorothia, Heterohelix, Globigerinelloides, Globotruncana, Globotruncanella, Globotruncanita, Laeviheterohelix, Muricohedbergella, Planoglobulina, Planoheterohelix, Pseudoguembelina, Pseudotextularia, Radotruncana, Rugoglobigerina, Rugotruncana and Schackoina. Most genera are typical of Late Cretaceous planktic foraminiferal fauna that were widespread in the Neo-Tethyan ocean. The co-occurred benthic foraminiferal genera include Ammobaculites, Cibicides, Lenticulina and Orbitolina.

These genera and species show temporal changes in the Chuangde Formation (CORBs) (Figures 3–10). Important bio-events (Figure 3) include (1) the last occurrence (LO) (S42) of *D. asymetrica*, (2) the first occurrence (FO) (S54) of *C. plmmerae*, (3) the first occurrence (FO) (S82) and (5) the last occurrence (LO) (S113) of *R. calcarata*.

The well-preserved planktic foraminifera assemblages recovered from the Chuangde Formation (CORBs) in the Zhangguo area of Gyangze have been systematically analyzed and classified into five distinct biozones based on the established planktic foraminiferal zonal scheme of Petrizzo et al. [28]. The biozonal framework, comprising the *Dicariella asymetrica*, *Globotruncanita elevata*, *Contusotruncana plummerae*, *Radotruncana calcarata*, and *Globotruncanella havaensis* zones, has been successfully applied to categorize the foraminiferal species identified within the study section, as illustrated in Figure 3. This zonation not only provides a robust biostratigraphic framework but also enhances our understanding of the paleoecological and paleoenvironmental conditions prevalent during the deposition of the Chuangde Formation (CORBs).

3.1.1. *Dicariella asymetrica* Zone

The *Dicariella asymetrica* Zone is a total range zone, defined by Postuma (1971) [25] as the stratigraphic interval of total range of the *Dicarinella asymetrica*. In Zhangguo, the top of this zone is defined by the LO of *Dicariella asymetrica* at S42 and the base is undetermined. Key planktic species include: *Archaeoglobigerina blowi*, *Bifarina bohemica*, *Contusotruncana fornicata*, *Dicariella asymetrica*, *D. concavata*, *Globigerinelloides ultramicra*, *Globotruncanita elevata*, *Globotruncanita stuartiformis*, *Muricohedbergella flandrini*, *Heterohelix moremani*, and *H. reussi*. This zone is dated as Santonian in age.

3.1.2. *Globotruncanita elevata* Zone

The *Globotruncanita elevata* Zone is a partial range zone, defined by Postuma (1971) [25] as the stratigraphic interval with *Globotruncanita elevata*, from the last occurrence (LO) of the *Dicarinella asymetrica* to the first occurrence (FO) of *Globotruncana ventricosa*, which is later replaced by *Contusotruncana plummerae* according to Petrizzo et al. (2011) [26]. In Zhangguo, the base of this zone is determined by the LO of *Dicarinella asymetrica* at S43 and the top is defined by the FO of *Contusotruncana plummerae* at S54. Key planktic species include: *Archaeoglobigerina blowi*, *Bifarina bohemica*, *Contusotruncana fornicata*, *Globigerinelloides prairiehillensis*, *G. ultramicra*, *Globotruncana arca*,

 doi:10.20944/preprints202504.1520.v1

G. bulloides, *G. linneiana*, *Globotruncanita elevata*, *Globotruncanita stuartiformis*, *Muricohedbergella flandrini*, *Heterohelix moremani*, *H. reussi* and *Radotruncana subspinosa.* This zone is dated as early Campanian in age.

3.1.3. *Contusotruncana plummerae* Zone

The *Contusotruncana plummerae* Zone is an interval zone defined by Petrizzo et al. (2011) [26] as the stratigraphic interval from the first occurrence (FO) of the nominal taxon and the FO of *R. calcarata*. In Zhangguo, the base of this zone is delineated by the FO of *C. plummerae* at S54 and the top is determined by the FO of *R. calcarata* at S82. Key planktic species include: *Archaeoglobigerina blowi*, *Bifarina bohemica*, *Contusotruncana fornicata*, *C. plummerae*, *Globigerinelloides prairiehillensis*, *G. ultramicra*, *Globotruncana arca*, *G. bulloides*, *G. linneiana*, *G. neotricarinata*, *Globotruncanita elevata*, *Globotruncanita stuartiformis*, *Muricohedbergella flandrini*, *Heterohelix moremani*, *H. reussi*, *Radotruncana subspinosa*, *Rugoglobigerina rugosa*, and *Schakoina multispinata*, etc. This zone is dated as middle Campanian in age.

3.1.4. *Radotruncana calcarata* Zone

Radotruncana calcarata (Cushman, 1927) [27], a globotruncanid planktonic foraminifer, is taxonomically debated, potentially assigned to *Radotruncana* (El-Naggar, 1971) [28], *Globotruncanita* (Reiss, 1957 [29]; emended by Robaszynski et al., 1984) [30], or *Globotruncana*. It is distinguished by its chamber spines (peripheral extensions of chambers along sutures by tapering tubolospines) (Longoria and VonFeldt, 1991; Wagreich et al., 2012) [31,32].

The *Radotruncana calcarata* Zone (TRZ, Herm, 1962) [33] is a globally recognized Late Campanian biozone, defined by the total range of *R. calcarata*. It spans low- to mid-latitude successions and is constrained to a brief interval (~806 kyr, 74.3/73.9–75.1/74.7 Ma; Wagreich et al., 2012) [31]. Initially misattributed to the Maastrichtian base in Tethyan sections (Caron, 1985) [34], it was later corrected to the Late Campanian (Schönfeld and Burnett, 1991) [35].

In Zhangguo, the base and top of this zone are marked by the FO of *R. calcarata* at S82 and the LO of *R. calcarata* in S113, respectively. Important planktic foraminiferal species include: *Archaeoglobigerina blowi*, *Bifarina bohemica*, *Contusotruncana fornicata*, *C. patelliformis*, *C. plicata*, *C. plummerae*, *Globigerinelloides prairiehillensis*, *G. ultramicra*, *Globotruncana arca*, *G. bulloides*, *Globotruncana falsostuarti*, *Globotruncana hilli*, *G. lapparenti*, *G. linneiana*, *Globotruncana lunaris*, *G. mariei*, *G. neotricarinata*, *G. ventricosa*, *Globotruncanita atlantica*, *G. elevata*, *G. pettersi*, *G. stuarti*, *G. stuartiformis*, *Muricohedbergella flandrini*, *Heterohelix carinata*, *H. cordites*, *H. globulosa*, *H. labellosa*, *H. moremani*, *H. navarroensis*, *H. planata*, *H. punctulata*, *H. reussi*, *H. striata*, *Laeviheterohelix dentata*, *Laeviheterohelix pulchra*, *Pseudoguemblina costulata*, *Pseudotextularia elegans*, *P. nuttalli*, *Pseudotextularia punctulata*, *Radotruncana calcarata*, *R. subspinosa*, *Rugoglobigerina rugosa*, and *Schakoina multispinata*, etc. The age of this zone is inferred as late Campanian.

3.1.5. *Globotruncanella havaensis* Zone

The *Globotruncanella havaensis* Zone is a partial range zone (PRZ) described by Caron (1978) [36], which spans the interval with *Globotruncanella havaensis* from the LO of *R. calcarata* to the first occurrence of *Globotruncana aegyptiaca.* In Zhangguo, the base of this zone is marked by the LO of *R. calcarata* at S113 and the top is undetermined. Important elements (planktic species) include: *Contusotruncana fornicata*, *C. patelliformis*, *Dorothia spheroidalis*, *Globigerinelloides prairiehillensis*, *Globotruncana arca*, *G. bulloides*, *G. forsostuarti*, *G. lapparenti*, *G. linneiana*, *G. ventricosa*, *Globotruncanita stuarti*, *G. stuartiformis*, *Globotruncanella havaensis*, *Heterohelix carinata*, *H. globulosa*, *H. navarroensis*, *H. reussi*, *H. striata*, *Laeviheterohelix dentata*, *L. pulchra* and others. The age of this zone is inferred as late Campanian.

Based on the foraminiferal biostratigraphy, the age of the CORBs of the Chuangde Formation in the study area should be within the Campanian.

 doi:10.20944/preprints202504.1520.v1

3.2. Microfacies Analysis

In this study, detailed microfacies analyses were performed on the Campanian strata, with a particular focus on the CORBs, exposed at the Zhangguo section in Gyangze and the Daba section in Kangmar. These sections are representative of the typical CORBs within the northern Tethyan Himalayan zone. Through comprehensive petrographic examination and paleontological analysis of thin sections, eight distinct microfacies (MF) have been distinguished from the study sections (Figures 11 and 12).

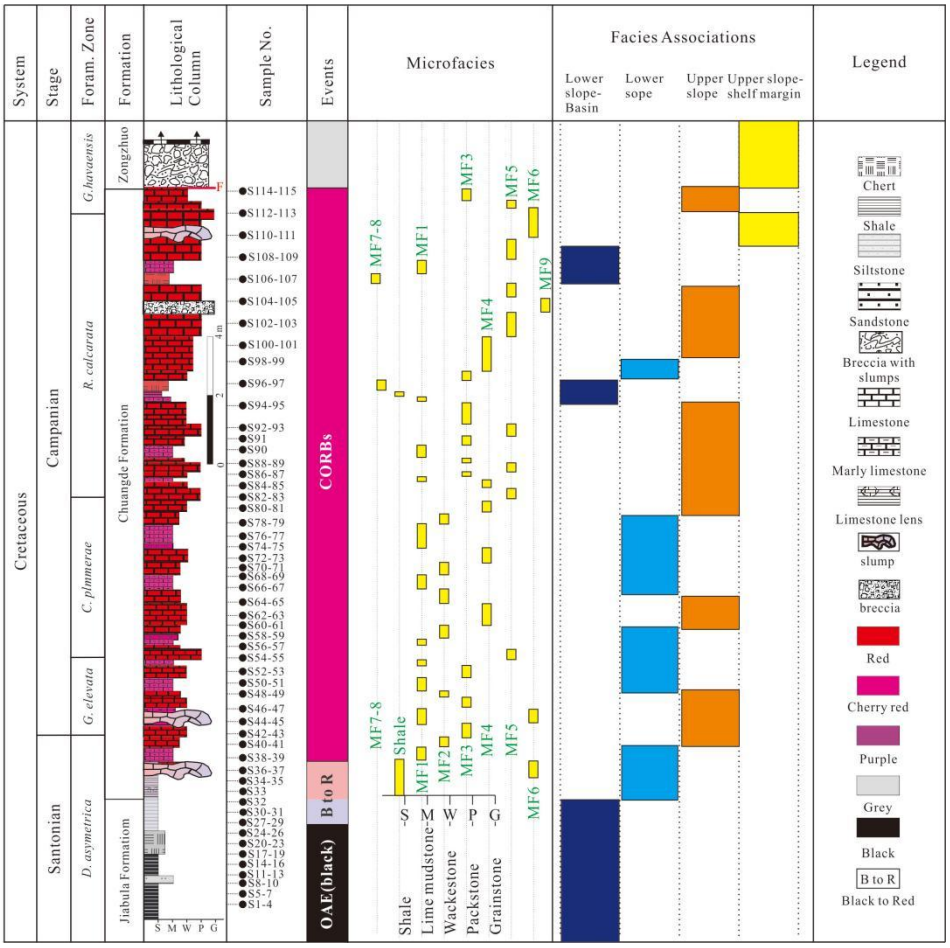

Figure 12. Temporal distribution of microfacies (MFs) and facies associations in the Zhangguo section.

3.2.1. MF1: Peloidal Marlstone

This microfacies is characterized by the presence of peloids, which are predominantly small (< 0.2 mm), sub-rounded to sub-angular microcrystalline grains. Genetically, these peloids are interpreted as fragmented pieces of carbonate mud, essentially small intraclasts. However, due to their diminutive size (<200 μm), they are classified within the peloid category (Figure 11A; S90). The poor sorting and the variability in grain morphology (ranging from sub-rounded to angular) suggest that these grains likely originated from the reworking of weakly lithified carbonate mud. The matrix, composed of lime mud and clay, indicates deposition in a low-energy environment. The peloids, although derived from higher-energy settings, were transported and deposited as suspension particles. Such depositional conditions are consistent with slope-basin environments situated in front of the shelf margin.

 doi:10.20944/preprints202504.1520.v1

3.2.2. MF2: Laminated Packed Wackestone

This microfacies is characterized by red laminated limestone, with laminae thickness ranging from 0.3 to 0.5 mm (Figures 11M and 11N). The red layers are rich in iron, primarily composed of hematite (Fe_2O_3), while the gray layers consist mainly of planktonic foraminiferal bioclasts and micritic calcite. This microfacies is predominantly observed in the lower (e.g., Figure 11M, sample S53) or upper (Figure 11N, sample S91) intervals of the Chuangde Formation in the Zhangguo section. The modern red iron-bearing carbonate mud in the Atlantis II Deep of the Red Sea is formed by the mixed deposition of hydrothermal iron and pelagic calcareous planktonic remains, with its depositional environment characterized by hydrothermal activity and oxidizing conditions. Based on lithofacies characteristics and modern sedimentary analogs, it is inferred that the formation environment and mechanism of the red laminated limestone in this microfacies are similar, likely representing an oxidizing deep-sea basin environment. The iron source may be related to submarine hydrothermal activity or terrigenous input, and the periodic alternation of laminae reflects cyclical changes in redox conditions or sedimentation rates.

3.2.3. MF3: Bioclastic Wackestone

This microfacies is characterized by a matrix-supported texture, with bioclasts comprising 10–30% of the rock volume, including planktonic foraminifers (Figures 11C and 11D). The abundance and composition of clasts exhibit significant variability at the centimeter scale. The heterogeneous sizes and shapes of bioclasts, combined with the matrix-supported fabric, indicate deposition in low-energy environments, likely below the fair-weather wave base or storm wave base. Within the study area, the Cretaceous Oceanic Red Beds (CORBs) of the Chuangde Formation, which are characterized by interbedded mudstone and limestone (e.g., samples S95 and S115), are representative of this microfacies.

3.2.4. MF4: Loosely Packed Wackestone

This microfacies shares similarities with MF3 but is distinguished by a higher proportion of bioclasts (30–50%) (Figure 11E; sample S85) and is typically expressed as thicker beds in outcrop. The texture is matrix-supported, with the interstitial space between grains often being smaller than the size of individual clasts. These characteristics suggest deposition in low-energy environments, likely with a significant supply of bioclasts derived from the upper water column.

3.2.5. MF5: Planktonic Foraminiferal Packstone

This microfacies is characterized by a grain-supported texture, predominantly composed of identifiable planktonic foraminifers (Figures 11G and 11J). The interstitial matrix consists of muddy material and microcrystalline cements, which account for approximately 25–50% of the rock volume (e.g., samples S110, S88). Based on its textural and compositional features, this microfacies is interpreted to have been deposited in either protected environments behind the shelf-margin shoal complex or in upper slope settings adjacent to the shoal complex.

3.2.6. MF6: Planktic Foraminiferal Grainstone

This microfacies is characterized by a grain-supported texture with microcrystalline calcite cement. The clasts are predominantly densely packed planktic foraminifers, accounting for >75% of the rock volume (Figures 11I and 11B). Notably, Figure 10I displays distinctive ‘pane fabric’ features. This microfacies is predominantly observed in the lower (e.g., sample S45; Figure 11I) and upper (e.g., sample S112; Figure 11B) intervals of the Chuangde Formation in the Zhangguo section, exhibiting a distinctive red coloration. Based on its textural and compositional attributes, this microfacies is interpreted to have been deposited in high-energy environments, likely within a shelf margin shoal complex or as grain flow deposits in slope settings.

 doi:10.20944/preprints202504.1520.v1

3.2.7. MF7: Radiolaria-Bearing Chert

This microfacies is characterized by a matrix of red cryptocrystalline quartz, with clasts predominantly composed of radiolarian tests (Figure 11P). The abundance of radiolarian clasts exhibits significant variability, ranging from approximately 1% to 30%. This microfacies is identified in the middle and upper Chuangde Formation of the Daba section in Kangmar, as well as in the upper part of the Chuangde Formation in Gyangze (Figure 12). The presence of this microfacies is indicative of a deep-water basin depositional environment, consistent with the pelagic conditions associated with the accumulation of radiolaria-bearing chert.

3.2.8. MF8: Radiolarian Chert

The matrix consists of red cryptocrystalline quartz, densely populated with radiolarian tests. This radiolarian chert is predominantly composed of planktonic radiolarians with siliceous skeletons, which are characteristic of deep-water environments located below the carbonate compensation depth (CCD) in the ocean. The radiolarian clasts are highly abundant, typically exceeding 30% and in some cases reaching up to 75%. This microfacies is identified in both the lower and upper Chuangde Formation of the Daba section in Kangmar (Figure 11Q), as well as in the upper part of the Chuangde Formation in the Zhangguo and Chuangde sections in Gyangze (Figure 12 and Figure 13B–C). These occurrences strongly corroborate the interpretation of a deep-water pelagic depositional environment for this microfacies.

3.2.9. MF9: Lithoclastic Wackestone/Floatstone

The matrix is predominantly composed of micrite, within which densely packed lithoclasts (floats) are embedded. Lithoclasts (floats) constitute over 60% of the rock volume, as evidenced by sample S104. Pressure solution stylolites, marked by arrows, are concentrated around the lithoclasts (floats) and are embedded within the micritic matrix. The fabric exhibits sutured laminated to sutured packed textures, indicative of significant compaction and diagenetic processes. This microfacies is observed in the upper part of the Chuangde Formation in the Zhangguo section in Gyangze.

The presence of lithoclastic wackestone/floatstone, characterized by high lithoclast content and pressure solution features, suggests a depositional environment influenced by gravitational transport and reworking of carbonate material. This is consistent with a deep-water slope setting, where sediment gravity flows, such as debris flows or turbidity currents, are common. The sutured fabric further supports a depositional environment subjected to significant overburden pressure, typical of slope or basinal settings. These features collectively reinforce the interpretation of a deep-water slope depositional environment for this microfacies.

Based on the microfacies characteristics (e.g., planktic foraminiferal packstone and grainstone) and microfossil assemblages (e.g., calcimicrobes, abundant planktic foraminiferal assemblages, silicimicrobes, and monotonous to paucispecific radiolarian assemblages), the planktic foraminiferal packstone and grainstone are interpreted to have been deposited in outer shelf to upper slope environments, proximal to the shelf margin shoal complex. In contrast, the radiolarian cherts are inferred to have accumulated in deep-water, oceanic basin environments situated below the carbonate compensation depth (CCD). This distinction highlights the contrasting depositional settings associated with these microfacies, reflecting the transition from shallower shelf-slope systems to deeper pelagic basins.

4. Discussion

The Chuangde Formation (CORBs) is a widely distributed stratigraphic unit in the northern Tethyan Himalaya that contains abundant planktic foraminiferal and/or radiolarian fossils. Biostratigraphically, the Chuangde Formation in southern Tibet has been previously assigned to a range from upper Santonian to Campanian/Maastrichtian, but the age of its topmost part is still in dispute (e.g., Wan et al., 2005; Li et al., 2011) [9,18].

 doi:10.20944/preprints202504.1520.v1

4.1. Facies Associations and Depositional Environments

Based on the integration of field observations and detailed microfacies analyses, the lithofacies of the upper Jiabula (Gyabula) Formation and the Chuangde Formation can be systematically classified into four distinct facies associations: (1) lower slope-basin, (2) lower slope, (3) upper slope, and (4) upper slope-shelf margin, as illustrated in Figures 12 and 13.

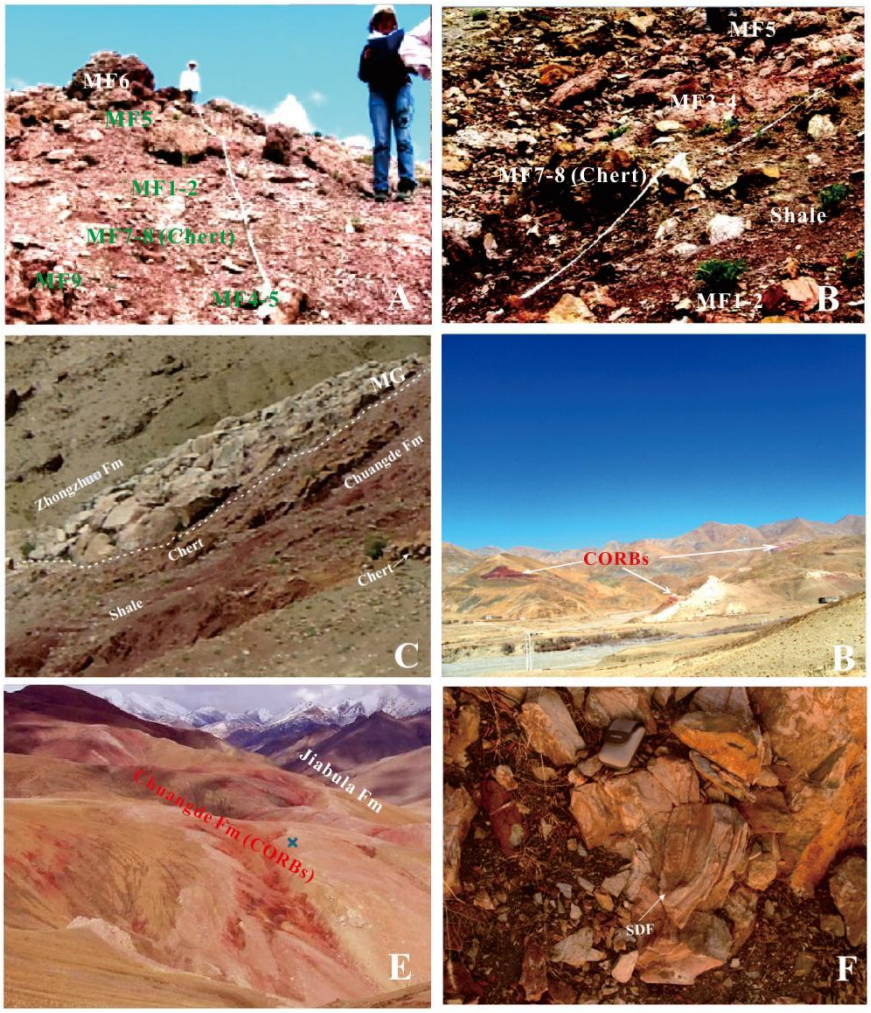

Figure 13. Field photos showing the combination of some lithofacies and sedimentary structures in the CORBs of the Gyangze—Kangmar basin.

(A) Microfacies (MF1–MF6) from the upper-near top part of the Chuangde Formation in the Zhangguo section, Gyangze (S100–S113 in Figure 12). (B) Microfacies (MF1–MF5) and cherts (MF7-8) from the upper part of the Chuangde Formation in the Zhangguo section, Gyangze (S94–S97 in Figure 12). (C) The erosional contact between megabreccias (MG) of the Zhongzhuo Formation and reddish shale and cherts of the Chuangde Formation from the Chuangde section in Gyangze. Notice that in this location, shales above the chert beds are removed by the megabreccia. (D) The exposure situation of Cretaceous oceanic red beds (BORBs) in the surrounding areas of Chuangde, Gyangze, with note: multiple repetitions of strata occur due to tectonic activities (folding and faulting). (E) Reddish shale and marlstone of the basal Chuangde Formation and its underlying Jiabula Formation from the Daba section in Kangmar. (F) Syn-depositional folds (SDF) in slump blocks of the middle Chuangde Formation, Gyangze.

The lower slope-basin facies association consists mainly of shale and marlstone (MF1), with occasional siltstone or radiolarian chert (MF7-8) interbeds (Figure 12). Within the upper Jiabula

 doi:10.20944/preprints202504.1520.v1

Formation (S1 to S25), this facies association is typified by black shales interbedded with cherts, which we interpret as indicative of deposition in basinal environments (Kneller and Branney, 1995; Stow and Johansson, 2000) [37,38]. This facies association is also identified in the upper (S94 to S97 and S106 to S109) Chuangde Formation (Figure 12 and Figure 13A–C), where it is manifested by laterally extensive, parallel-laminated red to cherry red shales, peloidal marlstone (MF1), and radiolarian cherts (MF7–8). The presence of radiolarian cherts (MF7 and MF8) in the upper Chuangde Formation may indicate basinal environments below the carbonate compensation depth (CCD).

The lower slope facies association is predominantly characterized by bioclastic wackestone with variable clast content (MF3-4), interbedded with shale layers, slump blocks, and breccias composed of foraminiferal grainstone (MF6). These facies exhibit a distinctive red to cherry red coloration and are primarily observed in the lower Chuangde Formation (Figure 12 and Figure 13C). In contrast to the basin facies, this association is marked by a higher proportion of carbonate components and, more significantly, the presence of slump blocks and breccias composed of grainstone. The foraminiferal grainstones are interpreted as having originated from the shelf margin and subsequently transported into slope environments via submarine slides or sheet-flow deposits (e.g., Mullins and Cook, 1986a, 1986b; Tucker and Wright, 1990) [39–41]. Notably, the slump blocks and breccias are relatively thin and infrequent, leading us to infer that they were deposited in distal or lower slope environments.

The upper slope facies association is predominantly characterized by bioclastic wackestone (MF3 and MF4) and slump blocks exhibiting brecciation (MF6), which are prominently observed within the middle-upper Chuangde Formation (Figure 12). The slump deposits display partial brecciation at their basal and frontal regions, while internally, they reveal syn-depositional folding structures (Figure 13F). Despite these localized deformations, the slump units maintain a remarkable lateral continuity, allowing them to be traced consistently across the outcrop scale. These features are interpreted as indicative of submarine slide events originating from the shelf margin, occurring within proximal or upper slope environments (e.g., Cook and Mullins, 1983; Mullins and Cook, 1986a, 1986b) [39,40,42].

The upper slope-shelf margin facies association is found in the near-top Chuangde Formation (S113 to S115; Figure 13A) and the basal Zongzhuo Formation (Figures 12 and 13C). In the upper Chuangde Formation, it primarily consists of foraminiferal wackestone (MF4) and packstone (MF5), with occasional internally deformed slump blocks (MF6). Alongside abundant planktonic foraminifera, a considerable number of benthic foraminifera (e.g., *Eouvigerina aculeata*, *Exsculptina* cf. *jacobi*, *Lenticulina* sp., *Miliammina* sp., *Neoflabellina* sp., and *Orbitolina* sp.) are present in both wackestones and packstones. The in situ packstone beds with benthic foraminifera suggest deposition near the shelf margin, close to the fair-weather or storm-wave base, while the slump blocks indicate upper slope environments where semi-consolidated sediments slid, fragmented, and moved basinward (Cook and Mullins, 1983) [42]. In the basal Zongzhuo Formation, this facies association is characterized by megabreccias (Figure 13C). The clasts in these megabreccias are composed of foraminiferal grainstones (MF6), but the megabreccias are matrix-supported, poorly sorted, and disorganized, often with erosional contacts with underlying shale or chert (e.g., Figure 13C). These megabreccias likely represent debris flow deposits in shelf margin-upper slope environments, formed by episodic shelf margin collapses (e.g., Mullins and Cook, 1986a, 1986b) [39,40].

4.2. Distribution and Age of the CORBs

The Late Cretaceous oceanic red beds (CORBs) are prominently developed across the North Tethys Himalaya (NTH) in southern Tibet, China, with intermittent exposures spanning from east to west in the regions of Yamdrok, Gyangze, Kangmar, Sagya, Angren, Gyirong, Zhongba, Zhada, and Zanskar (Figure 14). Regional stratigraphic correlations, based on lithologic associations and fossil assemblages (primarily planktic foraminifera and radiolaria), indicate that the ages of CORBs in this region exhibit significant spatial variability. Specifically, the CORBs in the Gyangze region are dated to the late Santonian to Campanian (Wan et al., 2005b) [43], while those in the Kangmar region span

 doi:10.20944/preprints202504.1520.v1

from the late Santonian to Maastrichtian (Li et al., 2011) [9], whereas in Gyirong, they extend from the Campanian to the Paleocene (Wan and Ding, 2002; Wan et al., 2005a, 2005b; Wang et al., 2017) [17,18,43,45], and the Zhada region records CORBs of early Paleocene age (Wan et al., 2005a) [18].

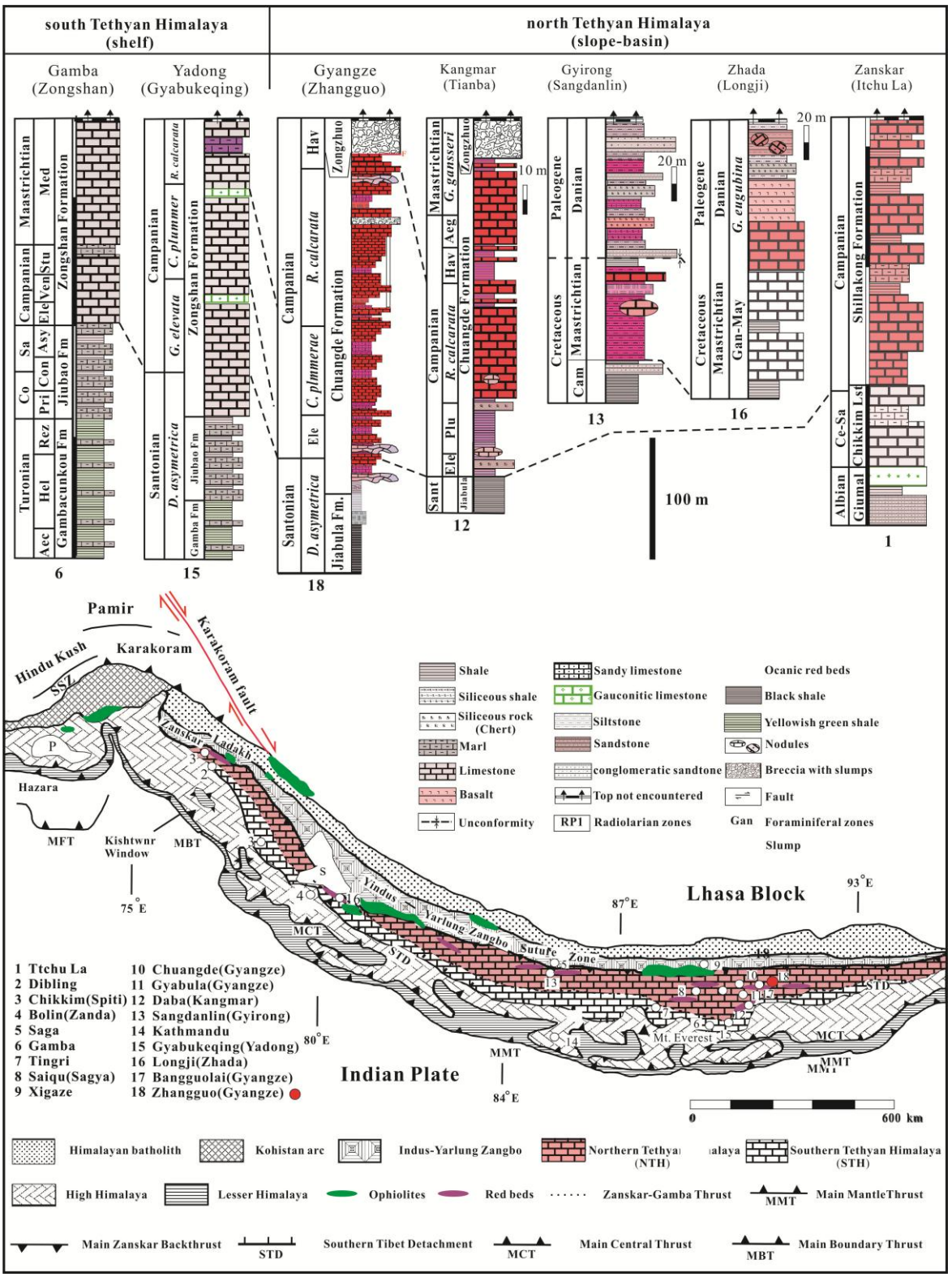

Figure 14. Distribution and stratigraphic correlation of the CORBs in Tethyan Himalayan area (after Gansser, 1964 [19]; Wan and Ding, 2002 [17]; Wan et al., 2005a [18], 2005b [43]; Li et al., 2011 [9]; Wang et al., 2017 [44]; Li et al., 2021 [5]; and this paper).

 doi:10.20944/preprints202504.1520.v1

A notable trend emerges in the age distribution of CORBs across the NTH, with a general tendency for younger ages towards the east. For instance, in Zanskar, Kangmar, and Gyangze, the CORBs are primarily Campanian, while in Gyirong and Zada/Zanda, they range from Maastrichtian to early Paleogene (Figure 14).

The depositional environments of the CORBs were traditionally interpreted as being confined to continental slope and deep basin settings, with their absence in shelf or shelf margin environments being widely accepted (e.g., Wan et al., 2005a, 2005c; Wang et al., 2005; Li et al., 2011) [4,9,18,43]. However, our study in the Gyangze region and adjacent areas reveals that CORBs are not limited to deep marine settings but instead occur across a broad spectrum of depositional environments, ranging from deep basins to slopes and even shelf settings (e.g., Figure 12). This finding aligns with the recent identification of shallow-marine, purple limestone beds within the upper Campanian Zongshan Formation in the Guru area of Yadong (Li et al., 2021) [5], which is tectonically situated within the Southern Tethys Himalaya (STH) (Figure 14).

Paleogeographic reconstructions further demonstrate that Campanian-aged CORBs were geographically extensive, spanning from shelf to basin environments (Figure 15). However, we emphasize that the thickness and temporal duration of the CORBs in different paleogeographic settings likely exhibit significant variability. This variability is primarily controlled by the extent to which Fe(II)-rich (or ferruginous) seawater infiltrated oxic depositional environments, highlighting the complex interplay between geochemical conditions and depositional processes during the Late Cretaceous.

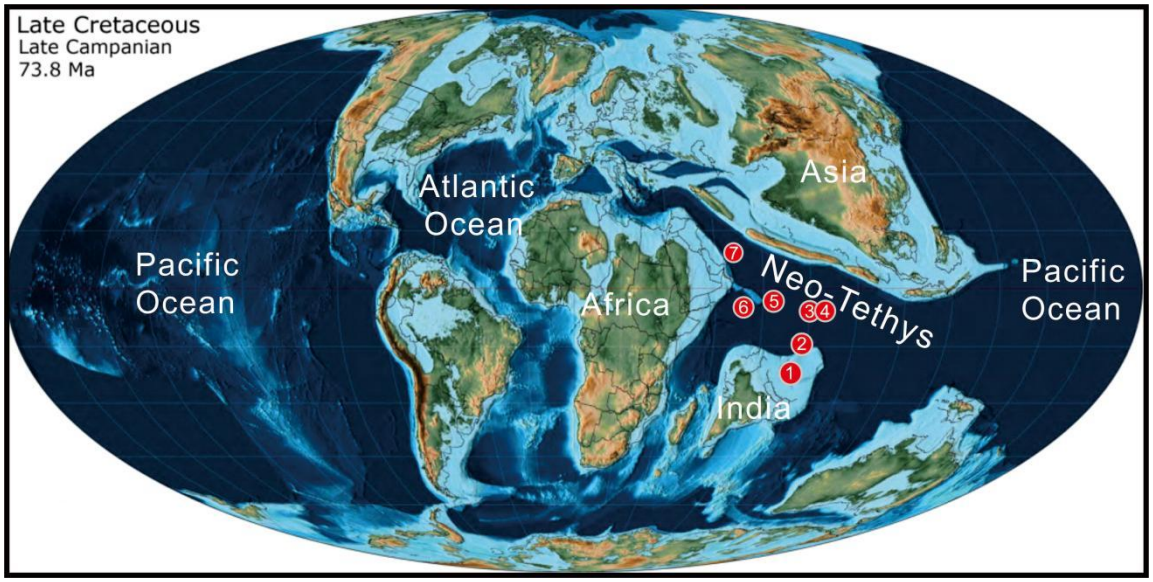

Figure 15. Late Campanian (~73.8 Ma) paleogeographic reconstruction and representative places of CORBs (discussed in the paper) in the Eastern Tethys. The location of continental blocks is modified from Scotese (2021) [20] using the on-line paleogeographic mapping tool for plate tectonic reconstructions (http://www.serg.unicam.it/Intro-Reconstr.html). Colors for paleogeographic reconstruction: brown—mountains; tan—highlands; yellow green—flatland; green—lowlands; light blue—shallow seas; blue—deep shelf; dark blue—deep ocean. Location of CORBs in the Eastern Tethys: ① Yadong (Gyabukeqing); ② Kangmar (Daba); ③ Gyangze (Bangguola); ④ Gyangze (Zhangguo); ⑤ Gyirong (Sangdanlin); ⑥ Zanda (Longji); ⑦ Zanskar (Itchu La).

5. Conclusions

This study presents a comprehensive analysis of foraminiferal biostratigraphy and microfacies from the Cretaceous oceanic red beds (CORBs) exposed in the Zhangguo section of Gyangze, southern Tibet, China. Five planktic foraminiferal biozones including *Dicarinella asymetrica*,

 doi:10.20944/preprints202504.1520.v1

Globotruncanita elevata, *Contusotruncana plummerae*, *Radotruncana calcarata*, and *Globotruncanella havaensis* were identified within the Chuangde Formation, confirming a Campanian age for these deposits (CORBs). Additionally, nine distinct microfacies were recognized, providing further insights into the depositional environments and processes. Integrating detailed field observations with microfacies analyses propose that the CORBs in the Gyangze region were deposited across a spectrum of environments, ranging from deep basin to slope and extending to shelf margin settings. Comparative analysis of the Gyangze CORBs with those from other sections in the Tethys Himalaya and globally suggests that many Campanian CORBs, particularly those in deep-sea environments, may have been deposited synchronously.

Author Contributions: For research articles with several authors, a short paragraph specifying their individual contributions must be provided. The following statements should be used "Conceptualization, Yuewei Li and Guobiao Li; methodology, Yuewei Li, Chengshan Wang, Guobiao Li; software, Yuewei Li; validation, Yuewei Li, Guobiao Li, Jie Ding and Mengmeng Jia; formal analysis, Yuewei Li, Guobiao Li and Dan Xie; investigation,Yuewei Li, Guobiao Li, Jie Ding,Tianyang Wang, Mengmeng Jia, Zhantu Baoke and Dan Xie; resources, Chengshan Wang and Guobiao Li; data curation, Yuewei Li and Guobiao Li; writing—original draft preparation, Yuewei Li, Guobiao Li,Jie Ding and Mengmeng Jia; writing—review and editing, Yuewei Li and Guobiao Li; visualization, Yuewei Li and Guobiao Li, Tianyang Wang; supervision, Chengshan Wang and Guobiao Li; project administration, Chengshan Wang and Guobiao Li; funding acquisition, Chengshan Wang and Guobiao Li. All authors have read and agreed to the published version of the manuscript."

Funding: This research was funded by the National Natural Science Foundation of China (grant number: 41972031, 41272030, 40972026), the Strategic Project of Science and Technology of Chinese Academy of Sciences (grant number: XDB050105003), and the National Basic Research Program of China (grant number: 2012CB822001).

Acknowledgments: The authors extend their gratitude to all individuals who participated in the field geological investigations related to this research and appreciate constructive comments from anonymous reviewers and the editors that greatly helped improve the manuscript significantly.

Conflicts of Interest: The authors declare no conflicts of interest.

Abbreviations

The following abbreviations are used in this manuscript:

CORBs	Cretaceous oceanic red beds
CCD	carbonate compensation depth
MRBs	marine red beds
CRBs	continental red beds
OAEs	Oceanic Anoxic Events
FO	first occurrence
LO	last occurrence
kyr	kilo years
Ma	Mega-annum
IGCP	International Geoscience Programme
Ce-Sa	Cenomanian-Santonian
Co	Conician
Sa	Satonian
Cam	Campanian
Arc	*Whiteinella archaeocretacea* zone
Hel	*Helvetoglobotruncana helvetica* zone
Rez	*Marginotruncana renzi* zone
Pri	*Dicarinella primitive* zone
Con	*Dicarinella concavata* zone
Asy	*Dicarinella asymetrica* zone

 doi:10.20944/preprints202504.1520.v1

Ele	*Globotruncanita elevata* zone
Ven	*Globotruncana ventricosa* zone
Stu	*Globotruncanita stuartiformis* zone
Med	*Globotruncanita elevata* zone
Plu	*Contusotruncana plummerae* zone
Hav	*Globotruncanella havanensis* zone
Aeg	*Globotruncana aegyptia* zone
Gan-May	*Gansserina gansseri* zone—*Abathomphalus mayaroensis* zone

Appendix A

List of taxa cited with author attributions and year of publication

Ammobaculites Cushman, 1910
Ammobaculites sp.
Ammobaculites kuzgongsuensis Hao, 1982
Archaeoglobigerina Pessagno, 1967
Archaeoglobigerina blowi (Pessagno Jr., 1967)
Bifarina Parker and Jones, 1972
Bifarina bohemica (Sulc, 1929)
Cibicides subtilis Zeng, 1982
Contusotruncana Korchagin, 1982
Contusotruncana sp.
Contusotruncana fornicata (Plummer, 1931)
Contusotruncana patelliformis (Gandolfi, 1955)
Contusotruncana plicata (White 1928)
Contusotruncana plummerae (Gandolfi, 1955)
Dicarinella Porthault, 1970
Dicarinella asymetrica (Sigal, 1952)
Dicarinella concavata (Brotzen, 1934)
Dorothia Plummer, 1931
Dorothia sp.
Dorothia spheroidalis Wan, 1985
Eouvigerina aculeata (Ehrenberg)
Exsculptina cf. *jacobi* (Marie)
Frondicularia Defrance, 1826
Frondicularia ? sp.
Globigerinelloides Cushman & Ten Dam, 1948
Globigerinelloides prairiehillensis (Pessagno Jr., 1967)
Globorotalites Brotzen, 1942
Globorotalites sp.
Globotruncana Cushman, 1927
Globotruncana arca (Cushman, 1926)
Globotruncana bulloides Vogler, 1941
Globotruncana falsostuarti Sigal, 1952
Globotruncana hilli Pessagno, 1967
Globotruncana lapparenti Brotzen, 1936
Globotruncana linneiana (d'Orbigny, 1839)
Globotruncana linneiana tricarinata (Quereau, 1893)
Globotruncana lunaris Masters, 1976
Globotruncana mariei Banner and Blow, 1960
Globotruncana neotricarinata (Micro-Unimin, 1983)
Globotruncana orientalis El Naggar 1966

 doi:10.20944/preprints202504.1520.v1

Globotruncana ventricosa White, 1928
Globotruncanella Reiss, 1957
Globotruncanella sp.
Globotruncanita Reiss, 1957
Globotruncanita atlantica (Caron, 1972)
Globotruncanita elevata (Brotzen, 1934)
Globotruncanita pettersi (Gandolf, 1955)
Globotruncanita stuarti (de Lapparent, 1918)
Globotruncanita stuartiformis (Dalbiez, 1955)
Globulina d'Orbigny, 1839
Gublerina acuta De Klasz, 1953
Guttulina sp. d'Orbigny, 1839
Heterohelix Ehrenberg, 1843
Heterohelix carinata (Cushman, 1938)
Heterohelix cordites Wan, 1985
Heterohelix globulosa (Ehrenberg, 1840)
Heterohelix labellosa (Nederbragt, 1991)
Heterohelix moremani (Cushman, 1938)
Heterohelix navarroensis Loeblich, 1951
Heterohelix planata (Cushman, 1938)
Heterohelix punctulata (Cushman, 1938)
Heterohelix reussi (Cushman, 1938)
Heterohelix striata (Ehrenberg, 1840)
Laeviheterohelix Nederbragt, 1990
Laeviheterohelix dentata (Stenestad, 1968)
Laeviheterohelix pulchra (Brotzen, 1936)
Lenticulina Lamarck, 1804
Lenticulina sp.
Miliammina Heron-Allen & Earland, 1930
Miliammina sp.
Muricohedbergella Brönnimann & Brown, 1958
Muricohedbergella flandrini Porthault, 1970
Muricohedbergella holmdelensis Olsson, 1964 (110)
Neoflabellina Bartenstein & Brand, 1951
Neoflabellina sp.
Orbitolina d'Orbigny, 1850
Orbitolina sp.
Planoglobulina Cushman, 1927
Planoglobulina carseyae (Plummer, 1931)
Planoglobulina sp.
Planulina d'Orbigny, 1826
Planulina sp.
Pseudoguembelina Brönnimann and Brown, 1953
Pseudoguembelina costellifera Masters, 1976
Pseudoguemblina costulata (Cushman, 1938)
Pseudotextularia Rzehak, 1891
Pseudotextularia sp.
Pseudotextularia elegans (Kikoine, 1891)
Pseudotextularia nuttalli (Voorwijk, 1937)
Pseudotextularia punctulata (Cushman, 1938)
Pyrulina d'Orbigny, 1839

 doi:10.20944/preprints202504.1520.v1

Pyrulina ? sp.
Pyrulinoides acuminata (d'Orbigny)
Radotruncana El-Naggar, 1971
Radotruncana calcarata (Cushman, 1927)
Radotruncana subspinosa (Pessagno, 1960)
Rhapydionina Stache, 1913
Rhapydionina sp.
Rugoglobigerina Brönnimann, 1952
Rugoglobigerina penny Brönnimann
Rugoglobigerina rugosa (Plummer, 1926)
Rugotruncana Brönnimann & Brown, 1956
Rugotruncana tilevi Brönnimann and Brown, 1956
Rugotruncana subcircumndifer (Gandolfi, 1955)
Rugotruncana cf. *subpennyi* (Gandolfi, 1955)
Schackoina Thalman, 1932
Schakoina multispinata (Cushman and Wickenden, 1930)
Sigalia Reiss, 1957
Sigalia decoratissima decoratissima (De Klasz, 1953)
Textularia Defrance, 1824
Textularia sp.

References

1. Turner, P. Continental Red Beds; Elsevier: Amsterdam, The Netherlands, 1980.
2. Fischer, A.G.; Arthur, M.A. Secular variations in the pelagic realm. SEPM Spec. Publ. 1977, 25, 19–50.
3. Basu, A. Continental red beds. Earth-Sci. Rev. 1982, 18, 186–188.
4. Wang, C.S.; Hu, X.M.; Sarti, M.; Scott, R.W.; Li, X.H. Upper Cretaceous oceanic red beds in southern Tibet: A major change from anoxic to oxic, deep-sea environments. Cretac. Res. 2005, 26, 21–32.
5. Li, Y.W.; Wang, C.S.; Li, G.B.; Xu, X.; Han, Z.C.; Elmes, M.; Wang, T.Y. Shallow-marine Cretaceous oceanic red beds from the southern Tethyan Himalaya, Tibet, western China: Biostratigraphy, microfacies analysis, and global correlations. Geol. J. 2021, 56, 6259–6287.
6. Lyell, C. Principles of Geology, Volume 3; John Murray: London, UK, 1833.
7. Jenkyns, H.C. Cretaceous anoxic events: from continents to oceans. J. Geol. Soc. Lond. 1976, 137, 171–188.
8. Arthur, M.A.; Schlanger, S.O.; Jenkyns, H.C. The Cenomanian-Turonian Oceanic Anoxic Event, II. Palaeoceanographic controls on organic-matter production and preservation. Geol. Soc. London Spec. Publ. 1987, 26, 401–420.
9. Li, G.B.; Jiang, G.G.; Wan, X.Q. The age of the Chuangde Formation in Kangmar, southern Tibet of China: Implications for the origin of Cretaceous oceanic red beds (CORBs) in the northern Tethyan Himalaya. Sediment. Geol. 2011, 235, 111–121.
10. Rong, J.Y.; Wang, Y.; Zhan, R.B.; Fan, J.X.; Huang, B.; Tang, P.; Li, Y.; Zhang, X.L.; Wu, R.C.; Wang, G.X. Silurian integrative stratigraphy and timescale of China (Review). Sci. China Earth Sci. 2019, 62, 89–111.
11. Wang, C.S.; Hu, X.M.; Huang, Y.J.; Scott, R.W.; Wagreich, M. Overview of Cretaceous oceanic red beds (CORBs): A window on global oceanic and climate change. SEPM Spec. Publ. 2009, 91, 13–33.
12. Štúr, D. Bericht über die geologische Uebersichts-Aufnahme des Wassergebietes der Waag und Neutra. Jahrb. Geol. Reichsanst. 1860, 11, 17–151.
13. Gümbel, C.W. Geognostische Beschreibung des bayerischen Alpengebirges und seines Vorlandes; J. Perthes: Gotha, Germany, 1861.
14. Wagreich, M.; Krenmayr, H.G. Upper Cretaceous oceanic red beds (CORBs) in the Northern Calcareous Alps (Austria): A review. Cretac. Res. 2005, 26, 21–30.
15. Mansour, A.; Wagreich, M. Earth system changes during the cooling greenhouse phase of the Late Cretaceous: Coniacian-Santonian OAE3 subevents and fundamental variations in organic carbon deposition. Earth-Sci. Rev. 2022, 229, 104022.

 doi:10.20944/preprints202504.1520.v1

16. Wang, C.; Hu, X.; Sarti, M.; Scott, R.W. Cretaceous oceanic red beds as a consequence of oceanic anoxic events. Sediment. Geol. 2011, 235, 27–37.
17. Wan, X.Q.; Ding, L. Discovery of the latest Cretaceous planktonic foraminifera from Gyirong of Southern Tibet and its chronostratigraphic significance. Acta Palaeontol. Sin. 2002, 41, 89–95.
18. Wan, X.Q.; Li, J.H.; Zhang, S.Z.; Wu, L.H. The Late Cretaceous–Paleocene Planktonic Foraminifera from Zanda, Western Tibet and Their Chronostratigraphic Implications. Acta Micropalaeontol. Sin. 2005a, 22, 10–18.
19. Gansser, A. Geology of the Himalayas; Wiley Interscience: London, UK, 1964; p. 289.
20. Scotese, R.C. An Atlas of Phanerozoic Paleogeographic Maps: The Seas Come In and the Seas Go Out. Annu. Rev. Earth Planet. Sci. 2021, 49, 679–728.
21. Dunham, R.J. Classification of carbonate rocks according to depositional texture. In Classification of Carbonate Rocks; Ham, W.E., Ed.; AAPG Mem. 1962, 1, 108–121.
22. Wilson, J.L. Carbonate Facies in Geologic History; Springer: New York, NY, USA, 1975.
23. Flügel, E. Mikrofazielle Untersuchungen in der alpinen Trias: Methoden und Probleme. Mitt. Ges. Geol. Bergbaustud. Österr. 1972, 21, 6–64.
24. Flügel, E. Microfacies of Carbonate Rocks: Analysis, Interpretation and Application, 2nd ed.; Springer: Berlin, Germany, 2010.
25. Postuma, J.A. Manual of Planktonic Foraminifera; Elsevier: Amsterdam, The Netherlands, 1971.
26. Petrizzo, M.R.; Falzoni, F.; Premoli Silva, I. Identification of the base of the lower-to-middle Campanian *Globotruncana ventricosa* Zone: Comments on reliability and global correlations. Cretac. Res. 2011, 32, 387–405.
27. Cushman, J.A. An outline of a re-classification of the foraminifera. Contrib. Cushman Lab. Foraminifer. Res. 1927, 3, 1–105.
28. El-Naggar, Z.R. On the classification, evolution, and stratigraphical distribution of the Globigerinacea. Proc. 2nd Planktonic Conf. 1971, 1, 421–461.
29. Reiss, Z. The Bilamellidea, nov. superfam., and remarks on Cretaceous globorotaliids. Contrib. Cushman Found. Foraminifer. Res. 1957, 8, 127–145.
30. Robaszynski, F.; Caron, M.; Gonzalez Donoso, J.M.; Wonders, A.H.; the European working group on Planktonic Foraminifera. Atlas of Late Cretaceous globotruncanids. Rev. Micropaleontol. 1984, 26, 145–305.
31. Longoria, J.F.; VonFeldt, A.E. Radotruncana calcarata (Cushman): A case of taxonomic confusion in the Globotruncanidae. J. Foraminifer. Res. 1991, 21, 234–241.
32. Wagreich, M. "OAE 3"–a low- to mid-latitude Atlantic oceanic event during the Coniacian-Santonian. Clim. Past Discuss. 2012, 8, 1209–1227.
33. Herm, D. Stratigraphische und miktopaläontologische Untersuchungen der Oberkreide im Lattengebirge und im Nierental. Abh. Bayer. Akad. Wiss. Math.-Naturwiss. Kl. 1962, 104, 1–119.
34. Caron, M. Cretaceous planktic foraminifera. In Plankton Stratigraphy; Bolli, H.M., Saunders, J.B., Perch-Nielsen, K., Eds.; Cambridge University Press: Cambridge, UK, 1985; pp. 17–86.
35. Schönfeld, J.; Burnett, J. Biostratigraphical correlation of the Campanian–Maastrichtian boundary: Lägerdorfe Henmoor (northwestern Germany); DSDP Sites 548A, 549 and 551 (eastern North Atlantic) with palaeobiogeographical and palaeoceanographical implications. Geol. Mag. 1991, 128, 479–503.
36. Caron, M. Cretaceous planktic foraminifers from DSDP Leg 40, Southeastern Atlantic Ocean. Initial Rep. Deep Sea Drill. Proj. 1978, 40, 651–678.
37. Kneller, B.C.; Branney, M.J. Sustained high-density turbidity currents and the deposition of thick massive sands. Sedimentology 1995, 42, 607–616.
38. Stow, D.A.V.; Johansson, M. Deep-water massive sands: nature, origin and hydrocarbon implications. Mar. Pet. Geol. 2000, 17, 145–174.
39. Mullins, H.T.; Cook, H.E. Carbonate apron models: alternatives to the submarine fan model for paleoenvironmental analysis and hydrocarbon exploration. Sediment. Geol. 1986, 48, 37–79.
40. Mullins, H.T.; Gardulski, A.F.; Hine, A.C. Catastrophic collapse of the west Florida carbonate platform margin. Geology 1986, 14, 167–170.

 doi:10.20944/preprints202504.1520.v1

41. Tucker, M.E.; Wright, V.P. Carbonate Sedimentology; Blackwell Scientific Publications: Oxford, UK, 1990; p. 482.
42. Cook, H.E.; Mullins, H.T. Basin margin. In Carbonate Depositional Environments; Scholle, P.A., Bebout, D.G., Moore, C.H., Eds.; AAPG Mem. 1983, 33, 539–617.
43. Wan, X.Q.; Li, G.B.; Si, J.L. The distribution and ages of Late Cretaceous-Paleocene oceanic red beds in southern Tibet. Earth Sci. Front. 2005b, 12, 31–37.
44. Wang, T. Y., Li G. B., Li, X. F., Niu, X. L. 2017. Early Eocene radiolarian fauna from the Sangdanlin, southern Tibet: constraints on the timing of initial India-Asia collision. Acta Geologica Sinica (English Edition), 91(6): 801–840.